

1 **A global analysis of reconstructed land climate changes during Dansgaard-** 2 **Oeschger events**

3 Mengmeng Liu^{1,2,*}, Iain Colin Prentice¹, Sandy P. Harrison²

4 1: Georgina Mace Centre for the Living Planet, Department of Life Sciences, Imperial College
5 London, Silwood Park Campus, Buckhurst Road, Ascot SL5 7PY, UK

6 2: Department of Geography and Environmental Science, University of Reading, Reading,
7 RG6 6AB, UK

8 *** Corresponding author: Mengmeng Liu (m.liu18@imperial.ac.uk)**

9 Ms for: *Climate of the Past*

10 **Abstract**

11 Dansgaard–Oeschger (D–O) warming events are comparable in magnitude and rate to the
12 anticipated 21st century warming. As such, they provide a good target for evaluation of the
13 ability of state-of-the-art climate models to simulate rapid climate changes. Despite the wealth
14 of qualitative information about climate changes during the D–O events, there has been no
15 attempt to date to make quantitative reconstructions globally. Here we provide reconstructed
16 changes of seasonal temperatures and plant-available moisture across multiple D–O events
17 between 50 and 30 ka based on available pollen records across the globe. These reconstructions
18 show that the largest warming occurred in northern extratropics, especially Eurasia, while
19 western North America and the southern extratropics were characterised by cooling. The
20 change in winter temperature was significantly larger than the change in summer temperature
21 in the northern extratropics and the tropics, indicating that the D–O warming events were
22 characterised by reduced seasonality, but there was no significant difference between the
23 summer and winter temperature changes in the southern extratropics. The antiphasing between
24 northern and southern extratropical changes, and the west-east pattern of cooling and warming
25 in North America were generally consistent across the eight D–O events examined, although
26 coherency is greatest during the strongest events. There was no globally consistent pattern
27 between changes in moisture and changes in temperature. These reconstructions can be used
28 to evaluate the spatial patterns of changes in temperature and moisture in the transient

29 simulations of the D-O events planned as part of the Palaeoclimate Modelling Intercomparison
30 Project.

31 1. Introduction

32 Dansgaard–Oeschger (D–O) events are characterised in Greenland by a transition from cold
33 Greenland Stadial (GS) to warmer Greenland Interstadial (GI) conditions (Dansgaard et al.,
34 1993). The surface air temperature in Greenland increased by 10–16° C during the warming
35 phases; these warming events occurred over an interval of between 50 and 200 years (Huber et
36 al., 2006; Kindler et al., 2014). Thus, the D-O events offer a parallel in terms of speed to
37 projected future warming, although both the baseline state and the mechanism inducing this
38 warming differ from anticipated 21st century climate changes. D-O events could therefore
39 provide an opportunity to determine how well climate models that are used for future
40 projections can simulate rapid climate changes (Malmierca-Vallet et al., 2023), particularly
41 regional patterns of warming (and cooling) that are regarded as a challenge for modelling
42 (Doblas-Reyes et al., 2021; Lee et al., 2021) and are highly important in assessing the
43 vulnerability of human societies to future climate changes (IPCC, 2022).

44 Although D-O events are found throughout the last glacial period, the largest number and the
45 most regular patterning occurred during Marine Isotope Stage 3 (MIS 3; 57 to 29 ka) when
46 there were 11 separate events (D-O 15 to D-O 5), while earlier stage such as MIS 4 (71 to 57
47 ka) only had 3 separate events (D-O 18 to 16). The typical duration of a cycle as manifested in
48 Greenland is *ca.* 1500 years and is characterised by an initial short slow warming, followed by
49 an abrupt large warming in matter of decades, followed by a long slow cooling over centuries
50 to millennia, with a terminal phase of fast cooling (e.g. D-O 8, D-O 12). However, there are
51 also cycles in which the warming and cooling phases took roughly the same time (e.g. D-O 5,
52 D-O 6, D-O 9). The magnitude of changes also differ, with both strong events (e.g. D-O 8, D-
53 O 12) and weak events (e.g. D-O 9).

54 The D-O signals are not just in Greenland – they are registered globally (Adolphi et al., 2018;
55 Corrick et al., 2020; Harrison and Sanchez-Goñi, 2010; Sánchez-Goñi et al., 2017; Voelker,
56 2002) and are reflected in changes in both temperature and precipitation. Both oceanic and ice-
57 core records indicate that temperature changes are out-of-phase between the northern and
58 southern hemispheres, and the southern hemisphere response both in terms of warming and
59 cooling phases is generally less abrupt (Dima et al., 2018; Vettoretti and Peltier, 2015). There
60 is a comparative lack of information from the continents about the manifestation of D-O events.
61 Shifts in vegetation types between GI and GS states have been interpreted as primarily a

62 temperature signal in the extratropics and a moisture signal in the tropics (Harrison and
63 Sanchez-Goñi, 2010). Speleothem records provide a good time-control on the synchronicity of
64 climate changes globally with the D-O events registered in Greenland (Adolphi et al., 2018;
65 Corrick et al., 2020), but the driver of this signal can either be temperature or precipitation
66 depending on the region. There are quantitative climate reconstructions based on terrestrial
67 pollen records from La Grande Pile (Guiot et al., 1993), Lago Grande di Monticchio (Huntley
68 et al., 1999), Padul (Camuera et al., 2022), El Cañizar de Villarquemado (Camuera et al., 2022;
69 Wei et al., 2021) and Lake Ohrid (Sinopoli et al., 2019), marine cores in the western
70 Mediterranean and offshore from Portugal (Sánchez-Goñi et al., 2002), diatom assemblages at
71 Les Echets, France (Ampel et al., 2010), chironomids from Lake Bergsee in central Europe
72 (Lapellegerie et al., 2024), bacterial membrane lipid records from the Eifel region (Zander et
73 al., 2024), isotopic measurements of earthworm calcite from the Rhine Valley (Prud'homme
74 et al., 2022) and clumped isotope measurements on snails in Hungary (Újvári et al., 2021).
75 Aside from the lack of comparable quantitative estimates from outside Europe, differences in
76 the methodology employed and in the specific climate variables reconstructed in each of these
77 studies limits their usefulness for model evaluation. In particular, given that there is still
78 uncertainty as to whether the D-O cycles are characterised by changes in seasonality such that
79 warming events are primarily driven by changes in winter (Flückiger et al., 2008; Zander et al.,
80 2024; Zumaque et al., 2025), in the regional strength of the warming (Harrison and Sanchez-
81 Goñi, 2010) and how warming relates to changes in moisture (Wei et al., 2021), there is a need
82 for more systematic reconstruction of seasonal climate changes.

83 In the paper, we provide reconstructed changes in seasonal temperatures and plant-available
84 moisture during the intervals corresponding to D-O warming events in Greenland between 50
85 and 30 ka based on available pollen records globally. We use a standard regression-based
86 approach to make the reconstructions. We analyse the regional patterns to identify key targets
87 for model evaluation.

88 **2. Methods**

89 **2.1. Data sources**

90 Modern pollen data were obtained from version 3 of the SPECIAL Modern Pollen Dataset
91 (SMPDSv3) (Harrison et al., 2025a). This global dataset was constructed by amalgamating and
92 standardising records from public repositories (e.g. Neotoma, Pangaea), existing regional

93 databases (e.g. European Modern Pollen Database, African Pollen Database), individual
94 publications and records provided by the original authors. The records were carefully screened
95 to remove duplicates that were present in more than one source. The modern samples were
96 obtained from multiple types of record, including pollen traps, surface samples, moss polsters
97 and different types of sediment, including cores from lakes and peatbogs, and section through
98 e.g. fluvial or loess deposits. In cases where the record was radiometrically dated, the database
99 preserves all samples younger than 50 yr B.P. However, some samples were undated and are
100 therefore recorded as modern if a collection date was given or assumed modern if not.

101 The dataset contains 26704 samples from 18202 different locations, and was created after
102 removing taxa that are not climatically diagnostic (e.g. obligate aquatics, carnivorous species,
103 cultivated plants). The dataset provides several levels of taxonomic aggregation; here we use
104 the most aggregated level, where woody species were generally combined at genus level and
105 herbaceous species at sub-family or family level unless they were palynologically distinctive,
106 occupied distinctive ecological niches and were sufficiently geographically widespread. This
107 "amalgamated" dataset contains relative abundance information for 1367 taxa. These samples
108 were aggregated by location (which is longitude, latitude and elevation) in order to remove
109 duplicates. Counts for *Quercus*, *Quercus* (deciduous) and *Quercus* (evergreen) were combined
110 because of inconsistent differentiation of *Quercus* pollen in different regional records.
111 Deciduous and evergreen oaks occupy different areas of climate space, particularly in terms of
112 seasonal moisture; specifically, evergreen oaks are typically found in areas characterised by
113 winter rainfall such as the Mediterranean. Nevertheless, since there are other plant taxa that are
114 similarly diagnostic of such regimes, the amalgamation of *Quercus* (deciduous) and *Quercus*
115 (evergreen) should not have a major effect on the robustness of our climate reconstructions.
116 We have tested this assumption by making reconstructions based on all taxa except *Quercus*
117 (Supplementary Materials, section 4). Taxa that occurred in less than 10 samples in the training
118 dataset were not used to make reconstructions because it is unlikely that the available samples
119 provided a reasonable estimate of the climate space occupied by these rare taxa (Liu et al.,
120 2020). After the location aggregation and the taxa filter, the dataset contains information on
121 18202 samples with relative abundance information for 609 taxa (Figure 1a).

122 We focus on three climate variables: mean temperature of the coldest month (MTCO), mean
123 temperature of the warmest month (MTWA), and a plant-available moisture index (α_{plant})
124 defined as the estimated ratio of actual to equilibrium evapotranspiration. These three variables

125 reflect ecophysiological controls on plant distribution (Harrison, 2020; Woodward, 1987) that
126 have been shown to independently influence the distribution and abundance of plant species
127 (Boucher-Lalonde et al., 2012; Wang et al., 2013; Wei et al., 2020). α_{plant} is a transformation
128 of the commonly used moisture index MI (defined as the estimated ratio of annual precipitation
129 to annual potential evapotranspiration) that emphasizes differences at the dry end of the climate
130 range, which have a more pronounced effect on vegetation distribution than differences at the
131 wet end (Prentice et al., 2017). Thus, α_{plant} can be better reconstructed from the pollen records
132 than MI.

133 The climate values at each SMPDSv3 site were obtained using a geographically-weighted
134 regression (GWR) of climatological values of mean monthly temperature, precipitation, and
135 fractional sunshine hours from the Climatic Research Unit Time-Series version 4.04 (CRU
136 TS4.04; Harris et al., 2020) dataset averaged over the period 1961–1990, which corresponds
137 to the interval from which most of the pollen samples were derived. GWR was to correct for
138 elevation differences between the CRU grid cells and the pollen sites. MTCO and MTWA were
139 taken directly from the GWR. MI was calculated for each site using SPLASH v1.0 (Davis et
140 al., 2017) based on daily values of precipitation, temperature and sunshine hours obtained using
141 a mean-conserving interpolation of the monthly values of each. MI was then transformed to
142 α_{plant} using the parametric Fu-Zhang formulation of the Budyko relationship (Supplementary
143 Materials, section 2). The climate space occupied by SMPDSv3 (Figure S1) samples a
144 reasonable range of global climate space and therefore should provide robust reconstructions
145 of climate changes under glacial conditions.

146 We use a global modern dataset for calibration of the pollen-climate relationships. The use of
147 a global dataset, rather than region-specific training data, relies on the principle of phylogenetic
148 niche conservatism (Harvey and Pagel, 1991; Qian and Ricklefs, 2004; Wang et al., 2025),
149 which states that traits tend to remain constant over time and that the climatic niches of specific
150 genera are also conservative (Harrison et al., 2025c). The use of a global dataset for calibration
151 makes it possible to sample a large range of climates, and thus makes it more likely that the
152 reconstructions of glacial climates are realistic and not confined to the limited climate range
153 sampled in any one region in modern times (Turner et al., 2020).

154 The Abrupt Climate Changes and Environmental Responses (ACER) database (Sánchez-Goñi
155 et al., 2017) was originally created to provide a source of pollen and charcoal data for Marine

156 Isotope Stage 3 (MIS 3), which includes 93 records with sufficient resolution and dating control
157 to detect sub-millennial scale variability. Much more records covering MIS 3 have become
158 available since the compilation of the ACER database, such as the synthetic pollen databases
159 available for Siberia (Cao et al., 2019, 2020) and China (Zhou et al., 2023) and the global
160 Legacy 2 dataset (Li et al., 2025), which can substantially cover the spatial gaps in the original
161 ACER database. We obtained these data from public sources or directly from the authors and
162 used them to create an update: ACER2 (Harrison et al., 2025b), which contains 233 additional
163 records covering some part or all of MIS 3 (note that the original ACER records are not
164 included in ACER2 due to licensing issue). The two datasets are combined in our analyses to
165 serve as the fossil pollen dataset (Supplementary Materials, section 3) to reconstruct the past
166 climates. We focus on the 279 records (253 terrestrial records and 26 marine records) between
167 50 and 30 ka (Figure 1b; Table 1). The fossil pollen data are taxonomically harmonised to be
168 consistent with the SMPDSv3.

169 **2.2. Climate reconstruction method**

170 We use fx -corrected Tolerance-weighted Weighted Averaging Partial Least Squares (fx TWA-
171 PLS: Liu et al., 2020, 2023) regression to derive the pollen-climate relationships in the modern
172 training dataset, and then apply these relationships to reconstruct past climates from the fossil
173 pollen records (Figure 2). fx TWA-PLS reduces the tendency of regression methods to compress
174 reconstructions towards the centre of the sampled climate range by applying a sampling
175 frequency correction to reduce the influence of uneven sampling of climate space and
176 weighting the contribution of individual taxa according to their climate tolerances (Liu et al.,
177 2020). Version 2 of fx TWA-PLS (fx TWA-PLSv2: Liu et al., 2023) uses P-splines smoothing
178 to derive the frequency correction and applies this correction both in estimating the climate
179 optima and tolerances, and in the regression itself, producing a further improvement in model
180 performance compared to fx TWA-PLSv1 (Liu et al., 2020).

181 We choose fx TWA-PLSv2 here. The evaluation is made by comparing the reconstructions made
182 using modern pollen data with modern climates using leave-out cross-validation, where one
183 site at a time is randomly selected as a test site and sites that are both geographically close
184 (within 50 km horizontal distance from the site) and climatically close (within 2% of the full
185 range of each climate variable in the dataset) are also removed from the training set, to prevent
186 redundancy in the climate information from inflating the cross-validation goodness of fit,
187 following Liu et al. (2020). This ensures that we are not just tuning to the training dataset, and

188 that we can reconstruct climates even when the training set does not completely cover the
 189 climate to be reconstructed because there are gaps in the climate space. Performance is assessed
 190 using R^2 and RMSEP (root-mean-square error of prediction), and compression is assessed
 191 using linear regression of the leave-out cross-validated reconstructions against the climate
 192 variable. The last significant number of components ($p \leq 0.01$) is selected to avoid overfitting
 193 due to the increase in the number of components. Reconstructions of MTCO, MTWA and α_{plant}
 194 are then made for every sample in each fossil record, using the last significant number of
 195 components. Sample-specific errors are estimated via bootstrapping (resampling the training
 196 set 1000 times) as described in Liu et al. (2020).

197 However, the low CO_2 at glacial period could lead to potential bias between reconstructed and
 198 actual plant-available moisture. Atmospheric CO_2 concentration has a direct impact on plant
 199 physiological processes, by modulating water-use efficiency (WUE), that is the ratio of carbon
 200 uptake to water loss through the stomata (Hatfield and Dold, 2019). The low CO_2 during the
 201 glacial period led to reduced water use efficiency (Farquhar, 1997; Gerhart and Ward, 2010;
 202 Prentice and Harrison, 2009). Statistical reconstructions cannot take this into account since
 203 they are based on modern relationships between pollen assemblages and climate under recent
 204 CO_2 levels (Bartlein et al., 2011; Chevalier et al., 2020). The actual conditions under low CO_2
 205 should be wetter than the vegetation-based reconstructions of moisture variables (Prentice et
 206 al., 2017, 2022a). Prentice et al. (2022a) provides a way of correction as follows:

$$207 \quad e(\text{MTGR}_1, \text{MI}_1, c_{a1}) = e(\text{MTGR}_0, \text{MI}_0, c_{a0}) \quad (1)$$

208 where e is the ratio of water loss to CO_2 uptake, a function of the mean temperature of the
 209 growing season (MTGR), moisture index (MI) and atmospheric CO_2 concentration (c_a). For
 210 MTGR and c_a , the subscript “1” denotes the past value, and the subscript “0” denotes the
 211 modern value. MI_0 is the reconstructed uncorrected past value, MI_1 is the “true” past value (to
 212 be estimated). The equation means that the “true” MI under past atmospheric conditions should
 213 produce the same e with the reconstructed uncorrected MI under modern atmospheric
 214 conditions, i.e. those pertaining to the modern pollen calibration dataset.

215 We transfer our reconstructed past α_{plant} back to the uncorrected moisture index MI_0 , and apply
 216 the CO_2 correction to obtain the actual moisture index MI_1 , then transfer it to actual plant-
 217 available moisture $\alpha_{\text{plant,corrected}}$ (Figure 2; Figures S2-1 & S2-2). Past and modern values of CO_2
 218 concentrations are taken from Bereiter et al. (2015), following Prentice et al. (2022a). Past

219 MTGR values are inferred by sinusoidal interpolation of reconstructed MTCO and MTWA,
220 assuming that the growing season corresponds to the period with temperatures $> 0^{\circ}\text{C}$. Modern
221 MTGR values are obtained using a geographically-weighted regression (GWR) of
222 climatological values (1961-1990) from the Climatic Research Unit Time-Series version 4.04
223 (CRU TS4.04; Harris et al., 2020) dataset averaged over the period 1961–1990, in order to
224 correct for elevation differences between the CRU grid cells and the fossil pollen sites. The
225 elevations of marine sites are set to 0 when applying GWR.

226 The CO_2 correction is implemented through the package COdos 0.0.2 (Prentice et al., 2022b)
227 with one modification, as follows. We found when applying the correction in cases where the
228 temperature reduction from modern was large ($> 5^{\circ}\text{C}$) that the use of different temperature
229 values to calculate the stomatal sensitivity term (ξ) and the compensation point (Γ^*) in the
230 correction algorithm sometimes produced an unrealistically large countervailing effect due to
231 the temperature difference alone. To avoid this problem, we calculate these physiological
232 quantities (ξ and Γ^*) using the mean of MTGR_1 and MTGR_0 .

233 **2.3. Age modelling of fossil records**

234 Both the ACER and ACER2 database provide age models for each pollen record. However,
235 the resolutions of the individual records are variable (ranging from 57 years to 13415 years)
236 and these age models are often imperfectly aligned with the dating of D-O warming events as
237 recorded in the Greenland ice core, and which have been shown to have a globally synchronous
238 imprint through analysis of speleothem records (Adolphi et al., 2018; Corrick et al., 2020). To
239 create a better alignment, we use dynamic time warping (DTW: Alshehri et al., 2019; Burstyn
240 et al., 2021; Giorgino, 2009) to adjust the age scale for each individual terrestrial record (Figure
241 2). Dynamic time warping optimises the similarity between two sequences (one “query” and
242 one “reference”) by stretching or compressing one sequence in the time dimension to match
243 the other. It adjusts the age scale without influencing the variable values, thus retaining the
244 original amplitude of change.

245 LOVECLIM simulation (Menviel et al., 2014) (covering the interval 50-30 ka) is currently the
246 only published simulation that has attempted to reproduce the specific timing and magnitude
247 of successive D-O cycles. It is coupled ocean-atmosphere-vegetation general circulation model
248 of intermediate complexity. The model was spun up to equilibrium using an initial atmospheric
249 CO_2 concentration of 207.5 ppm, orbital forcing appropriate for 50 ka BP, and an estimate of

250 the 50 ka BP ice-sheet orography and albedo obtained from an off-line ice-sheet model
251 simulation (Abe-Ouchi et al., 2007). After this initialization, the model was forced by time-
252 varying changes in orbital parameters, atmospheric trace gas concentrations and ice-sheet
253 configurations following Timm et al. (2008). In addition, meltwater pulses were added in the
254 North Atlantic in such a way as to reproduce observed sea-surface temperature (SST) variations
255 along the Iberian margin (Martrat et al., 2007). The simulations have proved adequate to
256 capture at least broad features of actual D-O events, and generally consistent with the
257 qualitative signals in Voelker (2002) compilation (Liu et al., 2022). We convert the age scale
258 of LOVECLIM simulations to the Antarctic Ice Core Chronology 2012 (AICC2012) time scale
259 (Veres et al., 2013).

260 We treat the mean annual temperature (MAT) calculated as the average of MTCO and MTWA
261 reconstructed from each individual fossil pollen record as the “query” time series, and find the
262 corresponding grid cell (the location of this fossil pollen record) in LOVECLIM simulations,
263 and use the simulated MAT at this grid cell as the “reference” time series. We further divide
264 each “query” and “reference” time series into discrete intervals using the mid-points between
265 the start dates of each D-O warming event as recorded in the Greenland ice core (Wolff et al.,
266 2010; converted into AICC2012 timescale), and normalize both time series in each interval to
267 remove the influence of differences in absolute values and the amplitude of changes. Then we
268 apply dynamic time warping to modify the time scale of the “query” to match the “reference”
269 in each interval. The adjusted age model for each fossil record is then applied to the
270 reconstructions of MTCO, MTWA, α_{plant} and $\alpha_{\text{plant,corrected}}$ from that record for subsequent
271 analyses.

272 **2.4. Assessment of regional climate changes during Greenland D-O warming events**

273 The magnitude of climate change during the interval corresponding to each D-O warming event
274 as registered in Greenland is calculated individually for each climate variable at each site. To
275 avoid making an assumption about the sign of the climate change at a site, we use a third-order
276 polynomial to fit the reconstructions during the interval from 300 years before to 600 years
277 after the official start date corresponding to Greenland D-O warming for each event (Wolff et
278 al., 2010; converted into AICC2012 timescale) to determine whether the change was positive
279 or negative. We then find the ages where this polynomial curve reaches the minimum and
280 maximum ($t_{\text{min,polynomial}}$ and $t_{\text{max,polynomial}}$). Since the smoothed polynomial may underestimate

281 or overestimate the amplitude of change, we use the reconstructions corresponding to
 282 $t_{\min, \text{polynomial}}$ and $t_{\max, \text{polynomial}}$ to obtain the changes (see Figure S3 for illustration). Whether it's
 283 an increasing or decreasing signal depends on whether $t_{\min, \text{polynomial}}$ occurs before or after
 284 $t_{\max, \text{polynomial}}$. The change of each climate variable (ΔV) is calculated as:

$$285 \quad \Delta V = V_{\text{end}} - V_{\text{start}} \quad (2)$$

286 where V_{start} is the reconstructed value at the start and V_{end} is the reconstructed value at the end
 287 of the event. The error of change ($\sigma_{\Delta V}$) is calculated using the following equation assuming
 288 V_{start} and V_{end} are independent:

$$289 \quad \sigma_{\Delta V} = \sqrt{\sigma_{V_{\text{end}}}^2 + \sigma_{V_{\text{start}}}^2} \quad (3)$$

290 where $\sigma_{V_{\text{start}}}$ is the sample-specific error of V_{start} and $\sigma_{V_{\text{end}}}$ is the sample-specific error of V_{end} .

291 To obtain the relationships between changes in different climate variables, we use a maximum
 292 likelihood method to estimate the ratio of ΔMTCO to ΔMTWA and the ratio of $\Delta \alpha_{\text{plant, corrected}}$
 293 to ΔMTWA to take account of the errors on both variables, following Liu et al. (2022).

294 As a measure of the accuracy of the DTW method to identify D-O events, we compare the
 295 number of identified events with the number of D-O events that should occur during the time
 296 covered by each record (Table 1). To assess whether events are missed in a particular record
 297 due to low sampling resolution, we examine the number of samples present in the 900-year
 298 interval covering the sampled D-O (i.e. 300 years before to 600 years after the official start
 299 date corresponding to Greenland D-O warming for each event), where low resolution is defined
 300 as ≤ 3 samples in this 900-year interval.

301 **3. Results**

302 fxTWA-PLS reproduces the modern climate reasonably well (Table 2; Figures S4-1 & 4-2).
 303 The performance is best for MTCO ($R^2 = 0.74$, RMSEP = 6.66, slope = 0.84) but is also good
 304 for MTWA ($R^2 = 0.60$, RMSEP = 3.63, slope = 0.72) and α_{plant} ($R^2 = 0.63$, RMSEP = 0.186,
 305 slope = 0.68). Assessment of the variance inflation factor scores shows that there is no problem
 306 of multicollinearity so that it is possible to reconstruct all three climate variables independently
 307 (Supplementary Table 1).

308 The use of dynamic time warping makes it possible to identify D-O events robustly (Figures
309 S5-1 to S5-8; Table 1; Supplementary Table 2). Some sites provide records in 50-30 ka but do
310 not cover the intervals of the D-O events; some marine sites are too far from the land to extract
311 GWR modern MTGR to apply CO₂ correction. Across the remaining 179 sites which should
312 have D-O events registered, we have identified 544 out of the 696 individual events (78 %). In
313 the majority of cases where a D-O event should have been registered but could not be identified
314 in an individual record (134 out of 152 cases), the resolution of that part of the record is
315 extremely poor.

316 ΔMTCO is found to be significantly larger than ΔMTWA in the northern extratropics and
317 tropics when considered across all D-O events and sites, indicating reduced seasonal contrast
318 between winter and summer temperatures; ΔMTCO is found to be larger than ΔMTWA , but
319 not significantly larger, in the southern extratropics (Figure 3; Table 3). There is no globally
320 consistent relationship between $\Delta\alpha_{\text{plant,corrected}}$ and ΔMTWA , although the positive relationship
321 in the tropics is marginally significant (Figure 4; Table 4).

322 The spatial patterns of ΔMTCO and ΔMTWA are generally consistent across multiple D-O
323 events (Figure 5), most noticeably that the largest warming occurs in Eurasia, while western
324 North America and the southern extratropics are characterised by cooling. These patterns are
325 also shown if only reconstructions where the change is twice the error of change are considered
326 (Figure S6), proving that the spatial patterns are robust to the choice of threshold. Nevertheless,
327 both the magnitude of the changes and the spatial patterns vary between the D-O events
328 (Figures S7-1 & S7-2). Strong events such as D-O 8 show more apparent changes (whether
329 warming or cooling), as well as a strong antiphasing between northern and southern
330 extratropical changes; while weak events such as D-O 9 show less apparent changes with
331 almost no north-south antiphasing (Figure 6).

332 The changes in plant-available moisture are less spatially coherent than the changes in
333 temperature (Figure 5). There is an increase in $\alpha_{\text{plant,corrected}}$ in some regions characterised by
334 warming, for example, southeastern China and Japan; but there are mixed signals of drying and
335 wetting in other regions characterised by warming, such as southern Europe. Furthermore,
336 regions characterised by cooling, such as western North America and southern extratropics,
337 can also show both drying and wetting. Changes in $\Delta\alpha_{\text{plant,corrected}}$ also show more variability
338 between D-O events than changes in temperature (Figure S7-4).

339 4. Discussion and Conclusions

340 4.1. Comparison with previous reconstructions

341 We have presented a first attempt to map the spatial patterns of quantitative changes in seasonal
342 temperatures and plant-available moisture during D-O events globally, using a consistent
343 methodology. These analyses show that there is an anti-phasing between changes in the
344 northern extratropics and the southern extratropics, with warming in the north and cooling in
345 the south. The largest and most consistent warming during D-O events occurs in Eurasia. There
346 is a significant difference between winter warming and summer warming in the northern
347 extratropics, resulting in an overall reduction in seasonality. Site-based reconstructions from
348 the Eifel region in central Europe, based on branched glycerol dialkyl glycerol tetraethers,
349 indicate minimal temperature changes during summer (Zander et al., 2024) and thus support
350 the idea that the D-O changes were driven by large changes in winter temperature. Zumaque
351 et al., (2025) provide seasonal temperature and precipitation reconstructions for 12 of the sites
352 from southern Europe (which are included in our fossil pollen records) but using the modern
353 analogue technique as the reconstruction method and the Eurasian Modern Pollen Database
354 version 2 (Davis et al., 2020) (EMPDv2; also included in our SMPDSv3) as the modern
355 training dataset. They show relatively stable summer temperatures but large change in MTCO
356 through the MIS3 D-O events, consistent with our reconstructions (using a regression-based
357 reconstruction method and a global modern training dataset) of a reduction in seasonality
358 during warming events in the northern extratropics. We find no significant difference in the
359 magnitude of seasonal warming in the southern extratropics. Since only quantitative
360 reconstructions of MAT (rather than MTCO and MTWA) are available from the southern
361 extratropics (e.g. Fletcher and Thomas, 2010; Newnham et al., 2017), there is no independent
362 confirmation of this result.

363 Qualitative interpretation of palaeo-records suggest that some many regions are characterised
364 by both warming and wetting, such as western Europe (Fletcher et al., 2010; Sánchez-Goñi et
365 al., 2008), eastern Europe (Fleitmann et al., 2009; Stockhecke et al., 2016), central Siberia
366 (Grygar et al., 2006), and the Great Basin USA (Denniston et al., 2007; Jiménez-Moreno et al.,
367 2010). Previous studies have also indicated drier conditions during D-O events, particularly in
368 parts of the USA such as the Pacific Northwest (Grigg and Whitlock, 2002) and Florida
369 (Grimm et al., 2006; Jiménez-Moreno et al., 2010). Our reconstructions show more mixed

370 signals and that there is no globally consistent relationship between changes in temperature
371 and moisture, either in regions characterised by warming or by cooling (Figure 4; Figure 5).
372 We have applied a correction for low CO₂ values during the glacial period to plant-available
373 moisture. The actual values ($\alpha_{\text{plant,corrected}}$) are generally higher than the vegetation-based
374 reconstructed values (α_{plant}) (Figure S2-1). However, the correction does not have a significant
375 impact on the spatial patterns during D-O events (Figure S2-2; Figure S7-3).

376 **4.2. Global training dataset vs local training dataset**

377 We have used a global pollen dataset for calibration of the pollen-climate relationships. In
378 general, reconstructions of glacial climates have used region-specific data sets (e.g. Dugerdil
379 et al., 2021, 2025; Newnham et al., 2017; Wei et al., 2021; Zumaque et al., 2025). Herzschuh
380 et al. (2023) made this explicit in their reconstructions of northern hemisphere climate over the
381 past 30,000 years, by restricting the modern training data to within a 2000 km radius of
382 individual fossil sites. The use of a region-specific training data set can be justified on the
383 grounds that it produces better statistics for the modern-day relationship between pollen
384 abundance and specific climate variables. Nevertheless, as pointed out by Chevalier et al.
385 (2020), an important issue is that the modern calibration data set has a span that adequately
386 samples the climate space experienced in the past. The use of a global dataset for calibration
387 makes it possible to sample a larger range of climates, and specifically to reconstruct climates
388 that might be very different from the modern range in that region. For example, reconstructions
389 of past European climate (Figure S8) based on region-specific training dataset would yield less
390 extreme winter temperatures than reconstructed using the global training data set. Although the
391 trend and spatial pattern might not be influenced greatly, the amplitude of change might be
392 underestimated.

393 The use of a global dataset, rather than region-specific training data, relies on the principle of
394 phylogenetic niche conservatism (Harvey and Pagel, 1991; Qian and Ricklefs, 2004; Wang et
395 al., 2025), which states that traits tend to remain constant over time. This also applies to the
396 climate niche (Crisp and Cook, 2012; Jiang et al., 2023; Peterson, 2011; Wiens et al., 2010;
397 Wiens and Graham, 2005) as evidenced by disjunct distributions of taxa across different
398 continents (Yin et al., 2021). Niche conservatism underpins the fact that the modern
399 distribution of specific genera can be predicted using climate-pollen relationships developed
400 from other regions (e.g. Huntley et al., 1989). However, the use of a global dataset can create

401 issues because of inconsistencies in taxonomic resolution between regions. The necessity for
402 treating all species of *Quercus* as a single taxon, despite the fact that evergreen and deciduous
403 species may occupy distinct climate niches in some regions, is a consequence of this. However,
404 we have shown (Supplementary Materials, section 4) that this has little impact on our
405 reconstructions – largely because the climatic distinction that would be conveyed through
406 separating deciduous and evergreen *Quercus* is also registered by the presence of other taxa.
407 Although the use of a global training dataset for climate reconstructions has not been a common
408 practice, it addresses the need to ensure that the modern training data adequately represents
409 past climate conditions and also facilitates making reconstructions for sites from regions with
410 limited modern pollen data.

411 **4.3. Targets for model evaluation**

412 The reconstructions in this paper can be used as targets for model evaluation, specifically the
413 two transient D-O experiments planned for the next phase of the Palaeoclimate Modelling
414 Intercomparison (see Malmierca-Vallet et al., 2023 for the experimental protocol). The first of
415 these experiments is a baseline simulation starting at 34 ka, a time with low obliquity, moderate
416 MIS3 greenhouse gas values, and an intermediate ice sheet configuration, which appears to be
417 most conducive to generating D-O like behaviour in climate models. The second experiment
418 involves the addition of freshwater, to examine whether this is necessary to precondition a state
419 conducive to generating D-O events. The anti-phasing in reconstructed temperature changes
420 between the northern and southern hemispheres is a general feature of climate model
421 experiments. Most models show larger warming in winter than in summer in the northern
422 hemisphere (e.g. Flückiger et al., 2008; Izumi et al., 2023; Van Meerbeeck et al., 2011), which
423 is also consistent with our reconstructions. However, the cooling in western North America
424 during D-O warming events in our reconstructions is not a feature of all climate model
425 simulations.

426 Models generally show an intensification of the northern hemisphere monsoons during D-O
427 events (e.g. Izumi et al., 2023; Menviel et al., 2020), but there is less consistency about changes
428 in plant-available moisture in the extratropics. Our reconstructions show an increase in
429 $\alpha_{\text{plant,corrected}}$ in southeastern China and Japan (Figure 5). Although $\alpha_{\text{plant,corrected}}$ is not a direct
430 reflection of summer precipitation, these changes are consistent with enhanced northern
431 hemisphere monsoons during D-O warming events, as shown by speleothem records from the
432 Caribbean (Warken et al., 2019) and speleothem and pollen records from Asia (Fohlmeister et

433 al., 2023; Wang et al., 2001; Zorzi et al., 2022). However, there are more spatial variability and
434 mixed signals.

435 The LOVECLIM model was used as a reference to adjust the age scale in the reconstructions
436 using MAT, but this does not preclude comparison of the seasonal temperatures. Here we
437 approximate the winter-season temperature as MTCO and summer-season temperature as
438 MTWA, since monthly temperatures are not available (only seasonal temperatures are available)
439 in LOVECLIM. The general spatial pattern of simulated changes in MTCO and MTWA (Figure
440 7) is consistent with the reconstructions, with largest warming in Eurasia, and cooling in the
441 southern extratropics. The simulated changes are strong during D-O 8 but weak during D-O 9
442 (Figures 9-1 & 9-2), again as shown by the reconstructions. However, there are important
443 differences. For example, simulated changes generally have smaller amplitude than shown by
444 the reconstructions, and the cooling over western North America is generally only in winter,
445 while the reconstructions show cooling over this region in both seasons. The relationship
446 between Δ MTCO and Δ MTWA is also different (Figure 8; Table 5): the simulated Δ MTCO is
447 shown to be significantly larger than Δ MTWA in the northern extratropics, but significantly
448 smaller than Δ MTWA in the southern extratropics, a contrast that is not so marked in the
449 reconstructions. This comparison illustrates the usefulness of the reconstructions for model
450 evaluation and to investigate the mechanisms that may not be adequately captured by current
451 models.

452 **4.4. Others**

453 Identifying D-O events in pollen records is often problematic, particularly in regions where
454 warming (especially if accompanied by dryer conditions) leads to a reduction (or an hiatus) in
455 sedimentation as reflected in the variable resolution of the available pollen records (e.g.
456 Camuera et al., 2022; Pini et al., 2022; Sinopoli et al., 2019; Wei et al., 2021). The use of
457 dynamic time warping goes some way to improving the identification of potential D-O events.
458 However, it precludes the calculation of a rate of change in climate. Thus, we have focused
459 here on the magnitude of the changes during specific warming events. It is also likely that some
460 of the variability in the reconstructed changes between different D-O events reflects imperfect
461 identification of specific events because of the comparatively modest resolution of the records.

462

463 **Data and code availability.** All the data used are public access and cited here. The code used
464 to generate the reconstructions and figures is available at [https://github.com/ml4418/DO-
climate-reconstruction-paper.git](https://github.com/ml4418/DO-
465 climate-reconstruction-paper.git) (will upload to zenodo in the final version).

466 **Author contributions.** ML, SPH and ICP designed the study. ML made the reconstructions
467 and produced the figures and tables. ML and SPH carried out the analyses. SPH wrote the first
468 draft of the paper and all authors contributed to the final draft.

469 **Competing Interests.** The authors declare not competing interests.

470 **Acknowledgements.** ML acknowledges support from Imperial College through the Lee
471 Family Scholarship. ICP acknowledges support from the ERC under the European Union
472 Horizon 2020 research and innovation programme (grant agreement no.: 787203 REALM).
473 SPH acknowledges fruitful discussions with colleagues from the D-O community working
474 group. We would like to acknowledge our colleagues who provided original pollen data for
475 inclusion in the ACER2 data set: Jon Camuera, Penelope González-Sampériz, Gonzalo
476 Jiménez-Moreno, Xinghi Liu, Rewi Newnham, Jian Ni, Roberta Pini, Cassie Rowe, Frank
477 Sirocco and María Del Socorro Lozano-García.

478

479

480 **References**

- 481 Abe-Ouchi, A., Segawa, T. and Saito, F.: Climatic conditions for modelling the Northern
482 Hemisphere ice sheets throughout the ice age cycle, *Clim. Past*, 3(3), 423–438,
483 doi:10.5194/cp-3-423-2007, 2007.
- 484 Adolphi, F., Bronk Ramsey, C., Erhardt, T., Edwards, R. L., Cheng, H., Turney, C. S. M.,
485 Cooper, A., Svensson, A., Rasmussen, S. O., Fischer, H. and Muscheler, R.: Connecting the
486 Greenland ice-core and U/Th timescales via cosmogenic radionuclides: testing the
487 synchronicity of Dansgaard–Oeschger events, *Clim. Past*, 14(11), 1755–1781, doi:10.5194/cp-
488 14-1755-2018, 2018.
- 489 Alshehri, M., Coenen, F. and Dures, K.: Effective sub-sequence-based dynamic time
490 warping, in *Artificial Intelligence XXXVI. SGAI 2019. Lecture Notes in Computer Science*,
491 edited by M. Bramer and M. Petridis, p. 11927, Springer, Cham., 2019.
- 492 Ampel, L., Bigler, C., Wohlfarth, B., Risberg, J., Lotter, A. F. and Veres, D.: Modest summer
493 temperature variability during DO cycles in western Europe, *Quat. Sci. Rev.*, 29(11), 1322–
494 1327, doi:10.1016/j.quascirev.2010.03.002, 2010.
- 495 Bartlein, P. J., Harrison, S. P., Brewer, S., Connor, S., Davis, B. A. S., Gajewski, K., Guiot,
496 J., Harrison-Prentice, T. I., Henderson, A., Peyron, O., Prentice, I. C., Scholze, M., Seppä, H.,
497 Shuman, B., Sugita, S., Thompson, R. S., Viau, A. E., Williams, J. and Wu, H.: Pollen-based
498 continental climate reconstructions at 6 and 21 ka: A global synthesis, *Clim. Dyn.*, 37(3),
499 775–802, doi:10.1007/s00382-010-0904-1, 2011.
- 500 Bereiter, B., Eggleston, S., Schmitt, J., Nehrbass-Ahles, C., Stocker, T. F., Fischer, H.,
501 Kipfstuhl, S. and Chappellaz, J.: Revision of the EPICA Dome C CO₂ record from 800 to
502 600 kyr before present, *Geophys. Res. Lett.*, 42(2), 542–549, doi:10.1002/2014GL061957,
503 2015.
- 504 Boucher-Lalonde, V., Morin, A. and Currie, D. J.: How are tree species distributed in
505 climatic space? A simple and general pattern, *Glob. Ecol. Biogeogr.*, 21(12), 1157–1166,
506 doi:10.1111/j.1466-8238.2012.00764.x, 2012.
- 507 Burstyn, Y., Gazit, A. and Dvir, O.: Hierarchical dynamic time warping methodology for
508 aggregating multiple geological time series, *Comput. Geosci.*, 150, 104704,

- 509 doi:10.1016/j.cageo.2021.104704, 2021.
- 510 Camuera, J., Ramos-Román, M. J., Jiménez-Moreno, G., García-Alix, A., Ilvonen, L., Ruha,
511 L., Gil-Romera, G., González-Sampériz, P. and Seppä, H.: Past 200 kyr hydroclimate
512 variability in the western Mediterranean and its connection to the African Humid Periods,
513 *Sci. Rep.*, 12(1), 9050, doi:10.1038/s41598-022-12047-1, 2022.
- 514 Cao, X., Tian, F., Andreev, A. A., Anderson, P. M., Lozhkin, A. V, Bezrukova, E. V, Ni, J.,
515 Rudaya, N., Stobbe, A., Wieczorek, M. and Herzsuh, U.: A taxonomically harmonized and
516 temporally standardized fossil pollen dataset from Siberia covering the last 40 ka [dataset
517 publication series], PANGAEA, doi:10.1594/PANGAEA.898616, 2019.
- 518 Cao, X., Tian, F., Andreev, A., Anderson, P. M., Lozhkin, A. V, Bezrukova, E., Ni, J.,
519 Rudaya, N., Stobbe, A., Wieczorek, M. and Herzsuh, U.: A taxonomically harmonized and
520 temporally standardized fossil pollen dataset from Siberia covering the last 40 kyr, *Earth*
521 *Syst. Sci. Data*, 12(1), 119–135, doi:10.5194/essd-12-119-2020, 2020.
- 522 Chevalier, M., Davis, B. A. S., Heiri, O., Seppä, H., Chase, B. M., Gajewski, K., Lacourse,
523 T., Telford, R. J., Finsinger, W., Guiot, J., Köhl, N., Maezumi, S. Y., Tipton, J. R., Carter, V.
524 A., Brussel, T., Phelps, L. N., Dawson, A., Zanon, M., Vallé, F., Nolan, C., Mauri, A., de
525 Vernal, A., Izumi, K., Holmström, L., Marsicek, J., Goring, S., Sommer, P. S., Chaput, M.
526 and Kupriyanov, D.: Pollen-based climate reconstruction techniques for late Quaternary
527 studies, *Earth-Science Rev.*, 210, 103384, doi:10.1016/j.earscirev.2020.103384, 2020.
- 528 Corrick, E. C., Drysdale, R. N., Hellstrom, J. C., Capron, E., Rasmussen, S. O., Zhang, X.,
529 Fleitmann, D., Couchoud, I. and Wolff, E.: Synchronous timing of abrupt climate changes
530 during the last glacial period, *Science* (80-.), 369(6506), 963 LP – 969,
531 doi:10.1126/science.aay5538, 2020.
- 532 Crisp, M. D. and Cook, L. G.: Phylogenetic niche conservatism: What are the underlying
533 evolutionary and ecological causes?, *New Phytol.*, 196(3), 681–694, doi:10.1111/j.1469-
534 8137.2012.04298.x, 2012.
- 535 Dansgaard, W., Johnsen, S. J., Clausen, H. B., Dahl-Jensen, D., Gundestrup, N. S., Hammer,
536 C. U., Hvidberg, C. S., Steffensen, J. P., Sveinbjörnsdottir, A. E., Jouzel, J. and Bond, G.:
537 Evidence for general instability of past climate from a 250-kyr ice-core record, *Nature*,

- 538 364(6434), 218–220, doi:10.1038/364218a0, 1993.
- 539 Davis, B. A. S., Chevalier, M., Sommer, P., Carter, V. A., Finsinger, W., Mauri, A., Phelps,
540 L. N., Zanon, M., Abegglen, R., Åkesson, C. M., Alba-Sánchez, F., Anderson, R. S.,
541 Antipina, T. G., Atanassova, J. R., Beer, R., Belyanina, N. I., Blyakharchuk, T. A., Borisova,
542 O. K., Bozilova, E., Bukreeva, G., Bunting, M. J., Clò, E., Colombaroli, D., Combourieu-
543 Nebout, N., Desprat, S., Di Rita, F., Djamali, M., Edwards, K. J., Fall, P. L., Feurdean, A.,
544 Fletcher, W., Florenzano, A., Furlanetto, G., Gaceur, E., Galimov, A. T., Gałka, M.,
545 Garcí\`ia-Moreiras, I., Giesecke, T., Grindean, R., Guido, M. A., Gvozdeva, I. G., Herzschuh,
546 U., Hjelle, K. L., Ivanov, S., Jahns, S., Jankovska, V., Jiménez-Moreno, G., Karpińska-
547 Kołaczek, M., Kitaba, I., Kołaczek, P., Lapteva, E. G., Latałowa, M., Lebreton, V., Leroy, S.,
548 Leydet, M., Lopatina, D. A., López-Sáez, J. A., Lotter, A. F., Magri, D., Marinova, E.,
549 Matthias, I., Mavridou, A., Mercuri, A. M., Mesa-Fernández, J. M., Mikishin, Y. A.,
550 Milecka, K., Montanari, C., Morales-Molino, C., Mrotzek, A., Muñoz Sobrino, C., Naidina,
551 O. D., Nakagawa, T., Nielsen, A. B., Novenko, E. Y., Panajiotidis, S., Panova, N. K.,
552 Papadopoulou, M., Pardoe, H. S., Pędziszewska, A., Petrenko, T. I., Ramos-Román, M. J.,
553 Ravazzi, C., Rösch, M., Ryabogina, N., Sabariego Ruiz, S., Salonen, J. S., Sapelko, T. V.,
554 Schofield, J. E., Seppä, H., Shumilovskikh, L., Stivrins, N., Stojakowits, P., Svobodova
555 Svitavska, H., Święta-Musznicka, J., Tantau, I., Tinner, W., Tobolski, K., Tonkov, S.,
556 Tsakiridou, M., et al.: The Eurasian Modern Pollen Database (EMPD), Version 2, *Earth Syst.*
557 *Sci. Data Discuss.*, 2020, 1–41, doi:10.5194/essd-2020-14, 2020.
- 558 Davis, T. W., Prentice, I. C., Stocker, B. D., Thomas, R. T., Whitley, R. J., Wang, H., Evans,
559 B. J., Gallego-Sala, A. V., Sykes, M. T. and Cramer, W.: Simple process-led algorithms for
560 simulating habitats (SPLASH v.1.0): Robust indices of radiation, evapotranspiration and
561 plant-available moisture, *Geosci. Model Dev.*, 10(2), 689–708, doi:10.5194/gmd-10-689-
562 2017, 2017.
- 563 Denniston, R. F., Asmerom, Y., Polyak, V., Dorale, J. A., Carpenter, S. J., Trodick, C., Hoye,
564 B. and González, L. A.: Synchronous millennial-scale climatic changes in the Great Basin
565 and the North Atlantic during the last interglacial, *Geology*, 35(7), 619–622,
566 doi:10.1130/G23445A.1, 2007.
- 567 Dima, M., Lohmann, G. and Knorr, G.: North Atlantic versus global control on Dansgaard-
568 Oeschger events, *Geophys. Res. Lett.*, 45(23), 12,912–991,998, doi:10.1029/2018GL080035,

569 2018.

570 Doblas-Reyes, F. J., Sörensson, A. A., Almazroui, M., Dosio, A., Gutowski, W. J., Haarsma,
571 R., Hamdi, R., Hewitson, B., Kwon, W.-T., Lamptey, B. L., Maraun, D., Stephenson, T. S.,
572 Takayabu, I., Terray, L., Turner, A. and Zuo, Z.: Linking global to regional climate change,
573 in *Climate Change 2021 – The Physical Science Basis: Working Group I Contribution to the*
574 *Sixth Assessment Report of the Intergovernmental Panel on Climate Change*, edited by V.
575 Masson-Delmotte, P. Zhai, A. Pirani, S. L. Connors, C. Péan, S. Berger, N. Caud, Y. Chen, L.
576 Goldfarb, M. I. Gomis, M. Huang, K. Leitzell, E. Lonnoy, J. B. R. Matthews, T. K. Maycock,
577 T. Waterfield, O. Yelekçi, R. Yu, and B. Zhou, pp. 1363–1512, Cambridge University Press,
578 Cambridge, United Kingdom and New York, NY, USA., 2021.

579 Dugerdil, L., Joannin, S., Peyron, O., Jouffroy-Bapicot, I., Vannière, B., Boldgiv, B.,
580 Unkelbach, J., Behling, H. and Ménot, G.: Climate reconstructions based on GDGT and
581 pollen surface datasets from Mongolia and Baikal area: calibrations and applicability to
582 extremely cold–dry environments over the Late Holocene, *Clim. Past*, 17(3), 1199–1226,
583 doi:10.5194/cp-17-1199-2021, 2021.

584 Dugerdil, L., Peyron, O., Ménot, G., Egamberdieva, D., Alimov, J., Leroy, S. A. G., Garnier,
585 E., Nowak, A. and Joannin, S.: First paleoenvironmental calibrations for modern pollen rain
586 of Tajikistan and Uzbekistan: A case study of pollen - vegetation functional biogeography of
587 Arid Central Asia, *Glob. Planet. Change*, 252, 104857, doi:10.1016/j.gloplacha.2025.104857,
588 2025.

589 Farquhar, G. D.: Carbon dioxide and vegetation, *Science* (80-.), 278(5342), 1411,
590 doi:10.1126/science.278.5342.1411, 1997.

591 Fleitmann, D., Cheng, H., Badertscher, S., Edwards, R. L., Mudelsee, M., Göktürk, O. M.,
592 Fankhauser, A., Pickering, R., Raible, C. C., Matter, A., Kramers, J. and Tüysüz, O.: Timing
593 and climatic impact of Greenland interstadials recorded in stalagmites from northern Turkey,
594 *Geophys. Res. Lett.*, 36(19), doi:10.1029/2009GL040050, 2009.

595 Fletcher, M.-S. and Thomas, I.: A quantitative Late Quaternary temperature reconstruction
596 from western Tasmania, Australia, *Quat. Sci. Rev.*, 29(17), 2351–2361,
597 doi:10.1016/j.quascirev.2010.06.012, 2010.

- 598 Fletcher, W. J., Sánchez-Goñi, M. F., Allen, J. R. M., Cheddadi, R., Combourieu-Nebout, N.,
599 Huntley, B., Lawson, I., Londeix, L., Magri, D., Margari, V., Müller, U. C., Naughton, F.,
600 Novenko, E., Roucoux, K. and Tzedakis, P. C.: Millennial-scale variability during the last
601 glacial in vegetation records from Europe, *Quat. Sci. Rev.*, 29(21), 2839–2864,
602 doi:10.1016/j.quascirev.2009.11.015, 2010.
- 603 Flückiger, J., Knutti, R., White, J. W. C. and Renssen, H.: Modeled seasonality of glacial
604 abrupt climate events, *Clim. Dyn.*, 31(6), 633–645, doi:10.1007/s00382-008-0373-y, 2008.
- 605 Fohlmeister, J., Sekhon, N., Columbu, A., Vettoretti, G., Weitzel, N., Rehfeld, K., Veiga-
606 Pires, C., Ben-Yami, M., Marwan, N. and Boers, N.: Global reorganization of atmospheric
607 circulation during Dansgaard–Oeschger cycles, *Proc. Natl. Acad. Sci.*, 120(36),
608 e2302283120, doi:10.1073/pnas.2302283120, 2023.
- 609 Gerhart, L. M. and Ward, J. K.: Plant responses to low [CO₂] of the past, *New Phytol.*,
610 188(3), 674–695, doi:10.1111/j.1469-8137.2010.03441.x, 2010.
- 611 Giorgino, T.: Computing and visualizing Dynamic Time Warping alignments in R: The dtw
612 package, *J. Stat. Softw.*, 31(7 SE-Articles), 1–24, doi:10.18637/jss.v031.i07, 2009.
- 613 Grigg, L. D. and Whitlock, C.: Patterns and causes of millennial-scale climate change in the
614 Pacific Northwest during Marine Isotope Stages 2 and 3, *Quat. Sci. Rev.*, 21(18), 2067–2083,
615 doi:10.1016/S0277-3791(02)00017-3, 2002.
- 616 Grimm, E. C., Watts, W. A., Jacobson, G. L., Hansen, B. C. S., Almquist, H. R. and
617 Dieffenbacher-Krall, A. C.: Evidence for warm wet Heinrich events in Florida, *Quat. Sci.*
618 *Rev.*, 25(17), 2197–2211, doi:10.1016/j.quascirev.2006.04.008, 2006.
- 619 Grygar, T., Kadlec, J., Pruner, P., Swann, G., Bezdička, P., Hradil, D., Lang, K., Novotna, K.
620 and Oberhänsli, H.: Paleoenvironmental record in Lake Baikal sediments: Environmental
621 changes in the last 160 ky, *Palaeogeogr. Palaeoclimatol. Palaeoecol.*, 237(2), 240–254,
622 doi:10.1016/j.palaeo.2005.12.007, 2006.
- 623 Guiot, J., de Beaulieu, J. L., Cheddadi, R., David, F., Ponel, P. and Reille, M.: The climate in
624 Western Europe during the last Glacial/Interglacial cycle derived from pollen and insect
625 remains, *Palaeogeogr. Palaeoclimatol. Palaeoecol.*, 103(1), 73–93, doi:10.1016/0031-
626 0182(93)90053-L, 1993.

- 627 Harris, I., Osborn, T. J., Jones, P. and Lister, D.: Version 4 of the CRU TS monthly high-
628 resolution gridded multivariate climate dataset, *Sci. Data*, 7, 109, doi:10.1038/s41597-020-
629 0453-3, 2020.
- 630 Harrison, S., Egbudom, M.-A. and Villegas-Diaz, R.: The SPECIAL Modern Pollen Data Set
631 for Climate Reconstructions, version 3 (SMPDSv3), , doi:10.17864/1947.001473, 2025a.
- 632 Harrison, S. P.: Climate reconstructions for the SMPDS v1 modern pollen data set, *Univ.*
633 *Read.*, doi:10.5281/zenodo.3605003, 2020.
- 634 Harrison, S. P. and Sanchez-Goñi, M. F.: Global patterns of vegetation response to
635 millennial-scale variability and rapid climate change during the last glacial period, *Quat. Sci.*
636 *Rev.*, 29(21), 2957–2980, doi:10.1016/j.quascirev.2010.07.016, 2010.
- 637 Harrison, S. P., Egbudom, M.-A. and Liu, M.: ACER2: The Abrupt Climate Changes and
638 Environmental Responses Database (version 2), , doi:10.17864/1947.001449, 2025b.
- 639 Harrison, S. P., Bartlein, P. J., Cruz-Silva, E., Haas, O., Jackson, S. T., Kaushal, N., Liu, M.,
640 Magri, D., Robson, D., Vettoretti, G. and Prentice, I. C.: Palaeoclimate perspectives on
641 contemporary climate change, *Ann. Rev. Environ. Resour.*, 50, 2025c.
- 642 Harvey, P. H. and Pagel, M. D.: *The comparative method in evolutionary biology*, Oxford
643 University Press., 1991.
- 644 Hatfield, J. L. and Dold, C.: Water-use efficiency: Advances and challenges in a changing
645 climate, *Front. Plant Sci.*, Volume 10, doi:10.3389/fpls.2019.00103, 2019.
- 646 Herzsuh, U., Böhmer, T., Li, C., Chevalier, M., Hébert, R., Dallmeyer, A., Cao, X.,
647 Bigelow, N. H., Nazarova, L., Novenko, E. Y., Park, J., Peyron, O., Rudaya, N. A., Schlütz,
648 F., Shumilovskikh, L. S., Tarasov, P. E., Wang, Y., Wen, R., Xu, Q. and Zheng, Z.:
649 LegacyClimate 1.0: a dataset of pollen-based climate reconstructions from 2594 Northern
650 Hemisphere sites covering the last 30 kyr and beyond, *Earth Syst. Sci. Data*, 15(6), 2235–
651 2258, doi:10.5194/essd-15-2235-2023, 2023.
- 652 Huber, C., Leuenberger, M., Spahni, R., Flückiger, J., Schwander, J., Stocker, T. F., Johnsen,
653 S., Landais, A. and Jouzel, J.: Isotope calibrated Greenland temperature record over Marine
654 Isotope Stage 3 and its relation to CH₄, *Earth Planet. Sci. Lett.*, 243(3), 504–519,

- 655 doi:10.1016/j.epsl.2006.01.002, 2006.
- 656 Huntley, B., Bartlein, P. J. and Prentice, I. C.: Climatic control of the distribution and
657 abundance of Beech (*Fagus L.*) in Europe and North America, *J. Biogeogr.*, 16(6), 551–560,
658 doi:10.2307/2845210, 1989.
- 659 Huntley, B., Watts, W. A., Allen, J. R. M. and Zolitschka, B.: Palaeoclimate, chronology and
660 vegetation history of the Weichselian Lateglacial: comparative analysis of data from three
661 cores at Lago Grande di Monticchio, southern Italy, *Quat. Sci. Rev.*, 18(7), 945–960,
662 doi:10.1016/S0277-3791(99)00007-4, 1999.
- 663 IPCC: Climate change 2022: Impacts, adaptation and vulnerability. Contribution of working
664 group II to the sixth assessment report of the Intergovernmental Panel on Climate Change,
665 edited by H.-O. Pörtner, D. C. Roberts, M. Tignor, E. S. Poloczanska, K. Mintenbeck, A.
666 Alegría, M. Craig, S. Langsdorf, S. Löschke, V. Möller, A. Okem, and B. Rama, Cambridge
667 University Press, Cambridge University Press, Cambridge, UK and New York, NY, USA.,
668 2022.
- 669 Izumi, K., Armstrong, E. and Valdes, P.: Global footprints of dansgaard-oeschger oscillations
670 in a GCM, *Quat. Sci. Rev.*, 305, 108016, doi:10.1016/j.quascirev.2023.108016, 2023.
- 671 Jiang, K., Wang, Q., Dimitrov, D., Luo, A., Xu, X., Su, X., Liu, Y., Li, Y., Li, Y. and Wang,
672 Z.: Evolutionary history and global angiosperm species richness–climate relationships, *Glob.*
673 *Ecol. Biogeogr.*, 32(7), 1059–1072, doi:10.1111/geb.13687, 2023.
- 674 Jiménez-Moreno, G., Anderson, R. S., Desprat, S., Grigg, L. D., Grimm, E. C., Heusser, L.
675 E., Jacobs, B. F., López-Martínez, C., Whitlock, C. L. and Willard, D. A.: Millennial-scale
676 variability during the last glacial in vegetation records from North America, *Quat. Sci. Rev.*,
677 29(21), 2865–2881, doi:10.1016/j.quascirev.2009.12.013, 2010.
- 678 Kindler, P., Guillevic, M., Baumgartner, M., Schwander, J., Landais, A. and Leuenberger,
679 M.: Temperature reconstruction from 10 to 120 kyr b2k from the NGRIP ice core, *Clim. Past*,
680 10(2), 887–902, doi:10.5194/cp-10-887-2014, 2014.
- 681 Lappelgerie, P., Millet, L., Rius, D., Duprat-Oualid, F., Luoto, T. and Heiri, O.: Chironomid-
682 inferred summer temperature during the Last Glacial Maximum in the Southern Black Forest,
683 Central Europe, *Quat. Sci. Rev.*, 345, 109016, doi:10.1016/j.quascirev.2024.109016, 2024.

- 684 Lee, J.-Y., Marotzke, J., Bala, G., Cao, L., Corti, S., Dunne, J. P., Engelbrecht, F., Fischer,
685 E., Fyfe, J. C., Jones, C., Maycock, A., Mutemi, J., Ndiaye, O., Panickal, S. and Zhou, T.:
686 Future global climate: Scenario-based projections and near-term information, in *Climate*
687 *change 2021: The physical science basis. Contribution of working group I to the sixth*
688 *assessment report of the Intergovernmental Panel on Climate Change*, edited by V. Masson-
689 Delmotte, P. Zhai, A. Pirani, S. L. Connors, C. Péan, S. Berger, N. Caud, Y. Chen, L.
690 Goldfarb, M. I. Gomis, M. Huang, K. Leitzell, E. Lonnoy, J. B. R. Matthews, T. K. Maycock,
691 T. Waterfield, O. Yelekçi, R. Yu, and B. Zhou, pp. 553–672, Cambridge University Press,
692 Cambridge, United Kingdom and New York, NY, USA., 2021.
- 693 Li, C., Ni, J., Böhmer, T., Cao, X., Zhou, B., Liao, M., Li, K., Schild, L., Wieczorek, M.,
694 Heim, B. and Herzschuh, U.: LegacyPollen2.0: an updated global taxonomically and
695 temporally standardized fossil pollen dataset of 3680 palynological records, ,
696 doi:10.1594/PANGAEA.965907, 2025.
- 697 Liu, M., Prentice, I. C., ter Braak, C. J. F. and Harrison, S. P.: An improved statistical
698 approach for reconstructing past climates from biotic assemblages, *Proc. R. Soc. A Math.*,
699 476(2243), 20200346, doi:10.1098/rspa.2020.0346, 2020.
- 700 Liu, M., Prentice, I. C., Menviel, L. and Harrison, S. P.: Past rapid warmings as a constraint
701 on greenhouse-gas climate feedbacks, *Commun. Earth Environ.*, 3, 196, doi:10.1038/s43247-
702 022-00536-0, 2022.
- 703 Liu, M., Shen, Y., González-Sampériz, P., Gil-Romera, G., ter Braak, C. J. F., Prentice, I. C.
704 and Harrison, S. P.: Holocene climates of the Iberian Peninsula: pollen-based reconstructions
705 of changes in the west–east gradient of temperature and moisture, *Clim. Past*, 19(4), 803–
706 834, doi:10.5194/cp-19-803-2023, 2023.
- 707 Malmierca-Vallet, I., Sime, L. C. and Members, the D. community: Dansgaard–Oeschger
708 events in climate models: Review and baseline Marine Isotope Stage 3 (MIS3) protocol,
709 *Clim. Past*, 19(5), 915–942, doi:10.5194/cp-19-915-2023, 2023.
- 710 Martrat, B., Grimalt, J. O., Shackleton, N. J., de Abreu, L., Hutterli, M. A. and Stocker, T. F.:
711 Four climate cycles of recurring deep and surface water destabilizations on the Iberian
712 margin, *Science (80-.)*, 317(5837), 502–507, doi:10.1126/science.1139994, 2007.

- 713 Van Meerbeeck, C. J., Renssen, H., Roche, D. M., Wohlfarth, B., Bohncke, S. J. P., Bos, J.
714 A. A., Engels, S., Helmens, K. F., Sánchez-Goñi, M. F., Svensson, A. and Vandenberghe, J.:
715 The nature of MIS 3 stadial–interstadial transitions in Europe: New insights from model–data
716 comparisons, *Quat. Sci. Rev.*, 30(25), 3618–3637, doi:10.1016/j.quascirev.2011.08.002,
717 2011.
- 718 Menviel, L., Timmermann, A., Friedrich, T. and England, M. H.: Hindcasting the continuum
719 of Dansgaard–Oeschger variability: Mechanisms, patterns and timing, *Clim. Past*, 10(1), 63–
720 77, doi:10.5194/cp-10-63-2014, 2014.
- 721 Menviel, L., Skinner, L. C., Tarasov, L. and Tzedakis, P. C.: An ice–climate oscillatory
722 framework for Dansgaard–Oeschger cycles, *Nat. Rev. Earth Environ.*, 1(12), 677–693,
723 doi:10.1038/s43017-020-00106-y, 2020.
- 724 Newnham, R. M., Alloway, B. V., Holt, K. A., Butler, K., Rees, A. B. H., Wilmshurst, J. M.,
725 Dunbar, G. and Hajdas, I.: Last Glacial pollen–climate reconstructions from Northland, New
726 Zealand, *J. Quat. Sci.*, 32(6), 685–703, doi:10.1002/jqs.2955, 2017.
- 727 Peterson, A. T.: Ecological niche conservatism: A time-structured review of evidence, *J.*
728 *Biogeogr.*, 38(5), 817–827, doi:10.1111/j.1365-2699.2010.02456.x, 2011.
- 729 Pini, R., Furlanetto, G., Vallé, F., Badino, F., Wick, L., Anselmetti, F. S., Bertuletti, P., Fusi,
730 N., Morlock, M. A., Delmonte, B., Harrison, S. P., Maggi, V. and Ravazzi, C.: Linking North
731 Atlantic and Alpine Last Glacial Maximum climates via a high-resolution pollen-based
732 subarctic forest steppe record, *Quat. Sci. Rev.*, 294, 107759,
733 doi:10.1016/j.quascirev.2022.107759, 2022.
- 734 Prentice, I. C. and Harrison, S. P.: Ecosystem effects of CO₂ concentration: evidence from
735 past climates, *Clim. Past*, 5(3), 297–307, doi:10.5194/cp-5-297-2009, 2009.
- 736 Prentice, I. C., Cleator, S. F., Huang, Y. H., Harrison, S. P. and Roulstone, I.: Reconstructing
737 ice-age palaeoclimates: Quantifying low-CO₂ effects on plants, *Glob. Planet. Change*, 149,
738 166–176, doi:10.1016/j.gloplacha.2016.12.012, 2017.
- 739 Prentice, I. C., Villegas-Diaz, R. and Harrison, S. P.: Accounting for atmospheric carbon
740 dioxide variations in pollen-based reconstruction of past hydroclimates, *Glob. Planet.*
741 *Change*, 211, 103790, doi:10.1016/j.gloplacha.2022.103790, 2022a.

- 742 Prentice, I. C., Villegas-Diaz, R. and Harrison, S. P.: COdos: CO2 correction tools, ,
743 doi:10.5281/zenodo.5083309, 2022b.
- 744 Prud'homme, C., Fischer, P., Jöris, O., Gromov, S., Vinnepand, M., Hatté, C., Vonhof, H.,
745 Moine, O., Vött, A. and Fitzsimmons, K. E.: Millennial-timescale quantitative estimates of
746 climate dynamics in central Europe from earthworm calcite granules in loess deposits,
747 *Commun. Earth Environ.*, 3(1), 267, doi:10.1038/s43247-022-00595-3, 2022.
- 748 Qian, H. and Ricklefs, R. E.: Geographical distribution and ecological conservatism of
749 disjunct genera of vascular plants in eastern Asia and eastern North America, *J. Ecol.*, 92(2),
750 253–265, doi:10.1111/j.0022-0477.2004.00868.x, 2004.
- 751 Sánchez-Goñi, M., Cacho, I., Turon, J., Guiot, J., Sierro, F., Peyrouquet, J., Grimalt, J. and
752 Shackleton, N.: Synchronicity between marine and terrestrial responses to millennial scale
753 climatic variability during the last glacial period in the Mediterranean region, *Clim. Dyn.*,
754 19(1), 95–105, doi:10.1007/s00382-001-0212-x, 2002.
- 755 Sánchez-Goñi, M. F., Landais, A., Fletcher, W. J., Naughton, F., Desprat, S. and Duprat, J.:
756 Contrasting impacts of Dansgaard–Oeschger events over a western European latitudinal
757 transect modulated by orbital parameters, *Quat. Sci. Rev.*, 27(11), 1136–1151,
758 doi:10.1016/j.quascirev.2008.03.003, 2008.
- 759 Sánchez-Goñi, M. F., Desprat, S., Danialu, A.-L., Bassinot, F. C., Polanco-Martínez, J. M.,
760 Harrison, S. P., Allen, J. R. M., Anderson, R. S., Behling, H., Bonnefille, R., Burjachs, F.,
761 Carrión, J. S., Cheddadi, R., Clark, J. S., Combourieu-Nebout, N., Mustaphi, J. C., Debussch, G. H.,
762 Dupont, L. M., Finch, J. M., Fletcher, W. J., Giardini, M., González, C., Gosling, W. D.,
763 Grigg, L. D., Grimm, E. C., Hayashi, R., Helmens, K., Heusser, L. E., Hill, T., Hope, G.,
764 Huntley, B., Igarashi, Y., Irino, T., Jacobs, B., Jiménez-Moreno, G., Kawai, S., Kershaw, A. P.,
765 Kumon, F., Lawson, I. T., Ledru, M.-P., Lézine, A.-M., Liew, P. M., Magri, D., Marchant,
766 R., Margari, V., Mayle, F. E., McKenzie, G. M., Moss, P., Müller, S., Müller, U. C.,
767 Naughton, F., Newnham, R. M., Oba, T., Pérez-Obiol, R., Pini, R., Ravazzi, C., Roucoux, K.
768 H., Rucina, S. M., Scott, L., Takahara, H., Tzedakis, P. C., Urrego, D. H., van Geel, B.,
769 Valencia, B. G., Vandergoes, M. J., Vincens, A., Whitlock, C. L., Willard, D. A. and
770 Yamamoto, M.: The ACER pollen and charcoal database: a global resource to document
771 vegetation and fire response to abrupt climate changes during the last glacial period, *Earth*
772 *Syst. Sci. Data*, 9(2), 679–695, doi:10.5194/essd-9-679-2017, 2017.

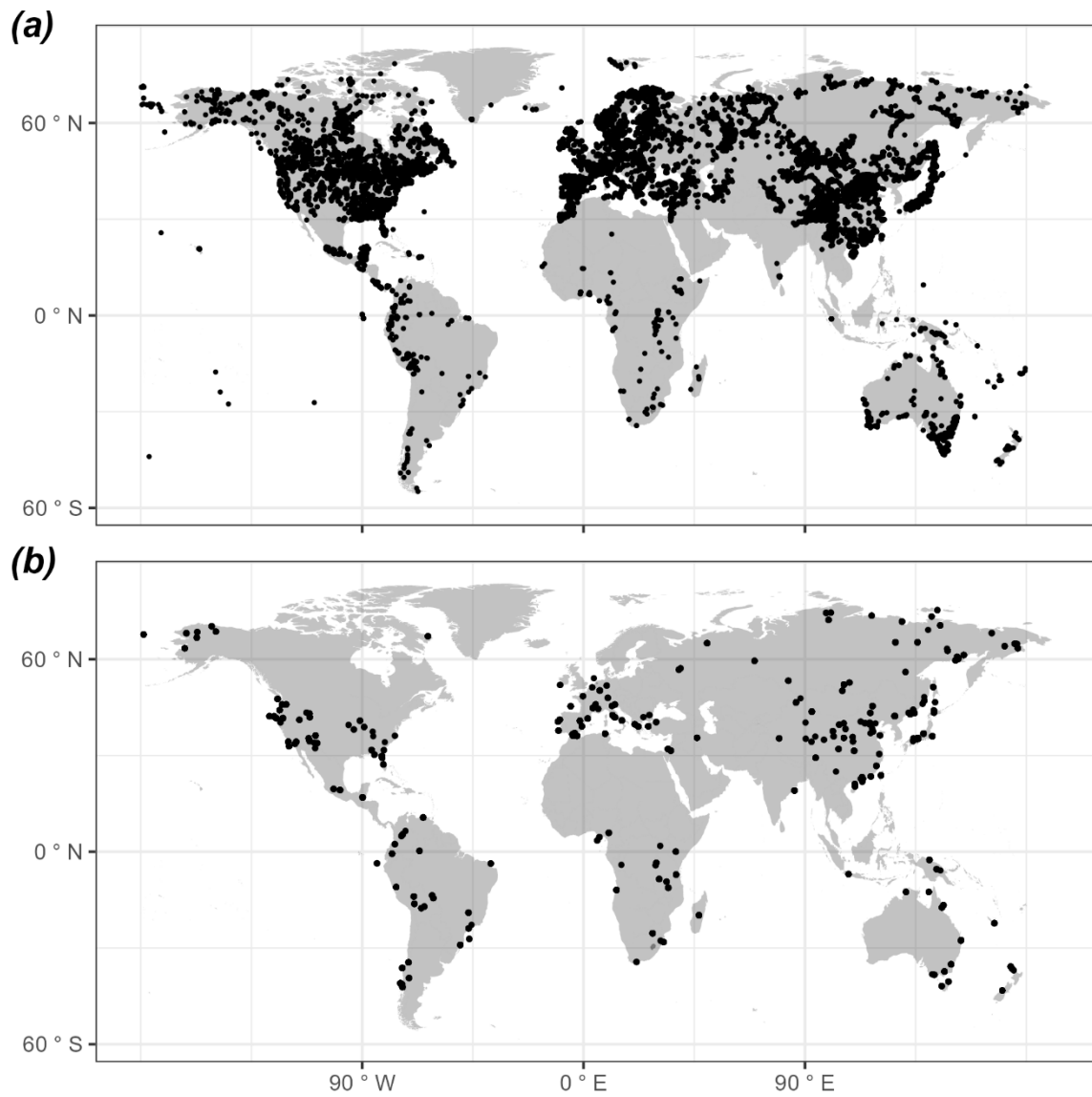
- 773 Sinopoli, G., Peyron, O., Masi, A., Holtvoeth, J., Francke, A., Wagner, B. and Sadori, L.:
774 Pollen-based temperature and precipitation changes in the Ohrid Basin (western Balkans)
775 between 160 and 70 ka, *Clim. Past*, 15(1), 53–71, doi:10.5194/cp-15-53-2019, 2019.
- 776 Stockhecke, M., Timmermann, A., Kipfer, R., Haug, G. H., Kwiecien, O., Friedrich, T.,
777 Menviel, L., Litt, T., Pickarski, N. and Anselmetti, F. S.: Millennial to orbital-scale variations
778 of drought intensity in the Eastern Mediterranean, *Quat. Sci. Rev.*, 133, 77–95,
779 doi:10.1016/j.quascirev.2015.12.016, 2016.
- 780 Timm, O., Timmermann, A., Abe-Ouchi, A., Saito, F. and Segawa, T.: On the definition of
781 seasons in paleoclimate simulations with orbital forcing, *Paleoceanography*, 23(2),
782 doi:10.1029/2007PA001461, 2008.
- 783 Turner, M. G., Wei, D., Prentice, I. C. and Harrison, S. P.: The impact of methodological
784 decisions on climate reconstructions using WA-PLS, *Quat. Res.*, 99, 341–356,
785 doi:10.1017/qua.2020.44, 2020.
- 786 Újvári, G., Bernasconi, S. M., Stevens, T., Kele, S., Páll-Gergely, B., Surányi, G. and
787 Demény, A.: Stadial-interstadial temperature and aridity variations in east central Europe
788 preceding the Last Glacial Maximum, *Paleoceanogr. Paleoclimatology*, 36(8),
789 e2020PA004170, doi:10.1029/2020PA004170, 2021.
- 790 Veres, D., Bazin, L., Landais, A., Toyé Mahamadou Kele, H., Lemieux-Dudon, B., Parrenin,
791 F., Martinerie, P., Blayo, E., Blunier, T., Capron, E., Chappellaz, J., Rasmussen, S. O.,
792 Severi, M., Svensson, A., Vinther, B. and Wolff, E. W.: The Antarctic ice core chronology
793 (AICC2012): An optimized multi-parameter and multi-site dating approach for the last 120
794 thousand years, *Clim. Past*, 9(4), 1733–1748, doi:10.5194/cp-9-1733-2013, 2013.
- 795 Vettoretti, G. and Peltier, W. R.: Interhemispheric air temperature phase relationships in the
796 nonlinear Dansgaard-Oeschger oscillation, *Geophys. Res. Lett.*, 42(4), 1180–1189,
797 doi:10.1002/2014GL062898, 2015.
- 798 Voelker, A. H. L.: Global distribution of centennial-scale records for Marine Isotope Stage
799 (MIS) 3: a database, *Quat. Sci. Rev.*, 21(10), 1185–1212, doi:10.1016/S0277-3791(01)00139-
800 1, 2002.
- 801 Wang, C., Wang, M., Zhu, S., Wu, X., Yang, S., Yan, Y. and Wen, Y.: Multiple ecological

- 802 niche modeling reveals niche conservatism and divergence in East Asian Yew (*Taxus*),
803 *Plants*, 14(7), doi:10.3390/plants14071094, 2025.
- 804 Wang, H., Prentice, I. C. and Ni, J.: Data-based modelling and environmental sensitivity of
805 vegetation in China, *Biogeosciences*, 10(9), 5817–5830, doi:10.5194/bg-10-5817-2013, 2013.
- 806 Wang, Y. J., Cheng, H., Edwards, R. L., An, Z. S., Wu, J. Y., Shen, C.-C. and Dorale, J. A.:
807 A high-resolution absolute-dated Late Pleistocene monsoon record from Hulu Cave, China,
808 *Science* (80-.), 294(5550), 2345–2348, doi:10.1126/science.1064618, 2001.
- 809 Warken, S. F., Scholz, D., Spötl, C., Jochum, K. P., Pajón, J. M., Bahr, A. and Mangini, A.:
810 Caribbean hydroclimate and vegetation history across the last glacial period, *Quat. Sci. Rev.*,
811 218, 75–90, doi:10.1016/j.quascirev.2019.06.019, 2019.
- 812 Wei, D., Prentice, I. C. and Harrison, S. P.: The climatic space of European pollen taxa,
813 *Ecology*, 101(8), e03055, doi:10.1002/ecy.3055, 2020.
- 814 Wei, D., González-Sampériz, P., Gil-Romera, G., Harrison, S. P. and Prentice, I. C.: Seasonal
815 temperature and moisture changes in interior semi-arid Spain from the last interglacial to the
816 Late Holocene, *Quat. Res.*, 101, 143–155, doi:10.1017/qua.2020.108, 2021.
- 817 Wiens, J. and Graham, C.: Niche conservatism: Integrating evolution, ecology, and
818 conservation biology, *Annu. Rev. Ecol. Evol. Syst.*, 36, 519–539,
819 doi:10.1146/annurev.ecolsys.36.102803.095431, 2005.
- 820 Wiens, J., Ackerly, D., Allen, A., Anacker, B., Buckley, L., Cornell, H., Damschen, E.,
821 Davies, J., Grytnes, J. A., Harrison, S., Hawkins, B., Holt, R., McCain, C. and Stephens, P.:
822 Niche conservatism as an emerging principle in ecology and conservation biology, *Ecol.*
823 *Lett.*, 13, 1310–1324, doi:10.1111/j.1461-0248.2010.01515.x, 2010.
- 824 Wolff, E. W., Chappellaz, J., Blunier, T., Rasmussen, S. O. and Svensson, A.: Millennial-
825 scale variability during the last glacial: The ice core record, *Quat. Sci. Rev.*, 29(21), 2828–
826 2838, doi:10.1016/j.quascirev.2009.10.013, 2010.
- 827 Woodward, F. I.: *Climate and Plant Distribution*, Cambridge University Press, Cambridge,
828 UK., 1987.
- 829 Yin, X., Jarvie, S., Guo, W.-Y., Deng, T., Mao, L., Zhang, M., Chu, C., Qian, H., Svenning,

- 830 J.-C. and He, F.: Niche overlap and divergence times support niche conservatism in eastern
831 Asia–eastern North America disjunct plants, *Glob. Ecol. Biogeogr.*, 30(10), 1990–2003,
832 doi:10.1111/geb.13360, 2021.
- 833 Zander, P. D., Böhl, D., Sirocko, F., Auderset, A., Haug, G. H. and Martínez-García, A.:
834 Reconstruction of warm-season temperatures in central Europe during the past 60 000 years
835 from lacustrine branched glycerol dialkyl glycerol tetraethers (brGDGTs), *Clim. Past*, 20(4),
836 841–864, doi:10.5194/cp-20-841-2024, 2024.
- 837 Zhou, B.-R., Liao, M.-N., Li, K., Xu, D.-Y., Chen, H.-Y., Ni, J., Cao, X.-Y., Kong, Z.-C.,
838 Xu, Q.-H., Zhang, Y., Herzsuh, U., Cai, Y.-L., Chen, B.-S., Chen, J.-A., Chen, L.-K.,
839 Cheng, B., Gao, Y., Huang, X.-Z., Li, S.-F., Li, W.-Y., Liu, K.-B., Liu, G.-X., Liu, P.-M.,
840 Liu, X.-Q., Ma, C.-M., Song, C.-Q., Sun, X.-J., Tang, L.-Y., Wang, M.-H., Wang, Y.-B., Xu,
841 J.-S., Yan, S., Yang, X.-D., Yao, Y.-F., Ye, C.-Y., Zhang, Z.-Y., Zhao, Z.-Y., Zheng, Z. and
842 Zhu, C.: A fossil pollen dataset of China, *Chinese J. Plant Ecol.*, 47(10), 1453–1463 [online]
843 Available from: <https://www.plant-ecology.com>, 2023.
- 844 Zorzi, C., Desprat, S., Clément, C., Thirumalai, K., Oliviera, D., Anupama, K., Prasad, S. and
845 Martinez, P.: When eastern India oscillated between desert versus savannah-dominated
846 vegetation, *Geophys. Res. Lett.*, 49(16), e2022GL099417, doi:10.1029/2022GL099417,
847 2022.
- 848 Zumaque, J., de Vernal, A., Fréchette, B., Guiot, J., Sánchez-Goñi, M. F., Barhoumi, C.,
849 Peyron, O., Peros, M., Burke, A., Camuera, J., Jiménez-Moreno, G. and Ramos-Román, M.
850 J.: Decoupled winter and summer climate changes in southern Europe during the Dansgaard-
851 Oeschger cycles, *Quat. Sci. Rev.*, 359, 109273, doi:10.1016/j.quascirev.2025.109273, 2025.
- 852

853 **Figures and Tables**

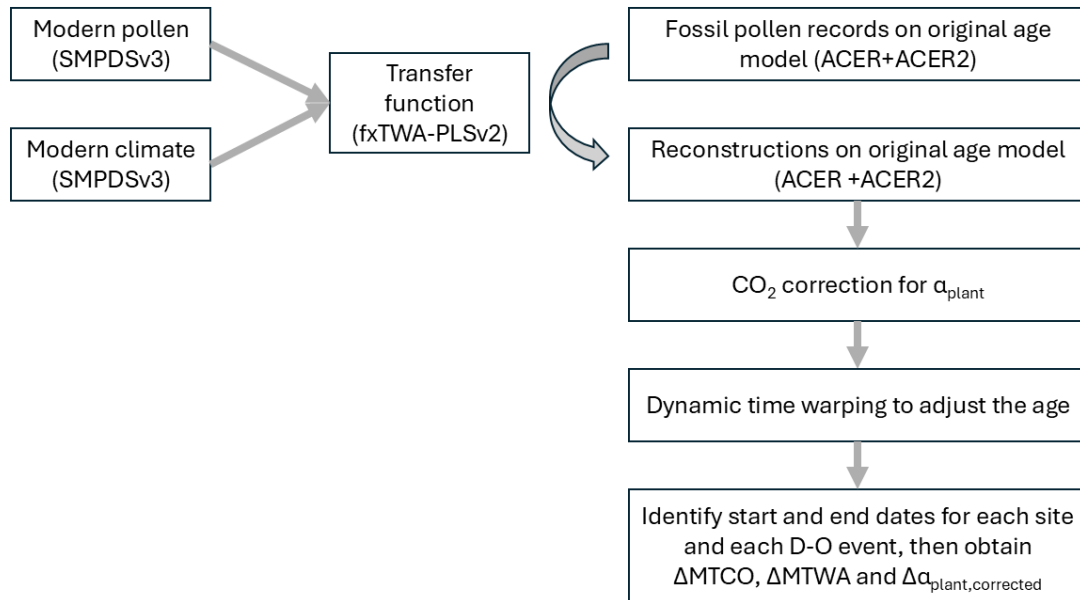
854 Figure 1: Map showing the locations of (a) modern pollen records used to derive the pollen-
855 climate transfer functions, and (b) fossil pollen records covering the interval 50-30 ka used for
856 the climate reconstructions.



857

858

859 Figure 2: Flow chart showing the methodology.



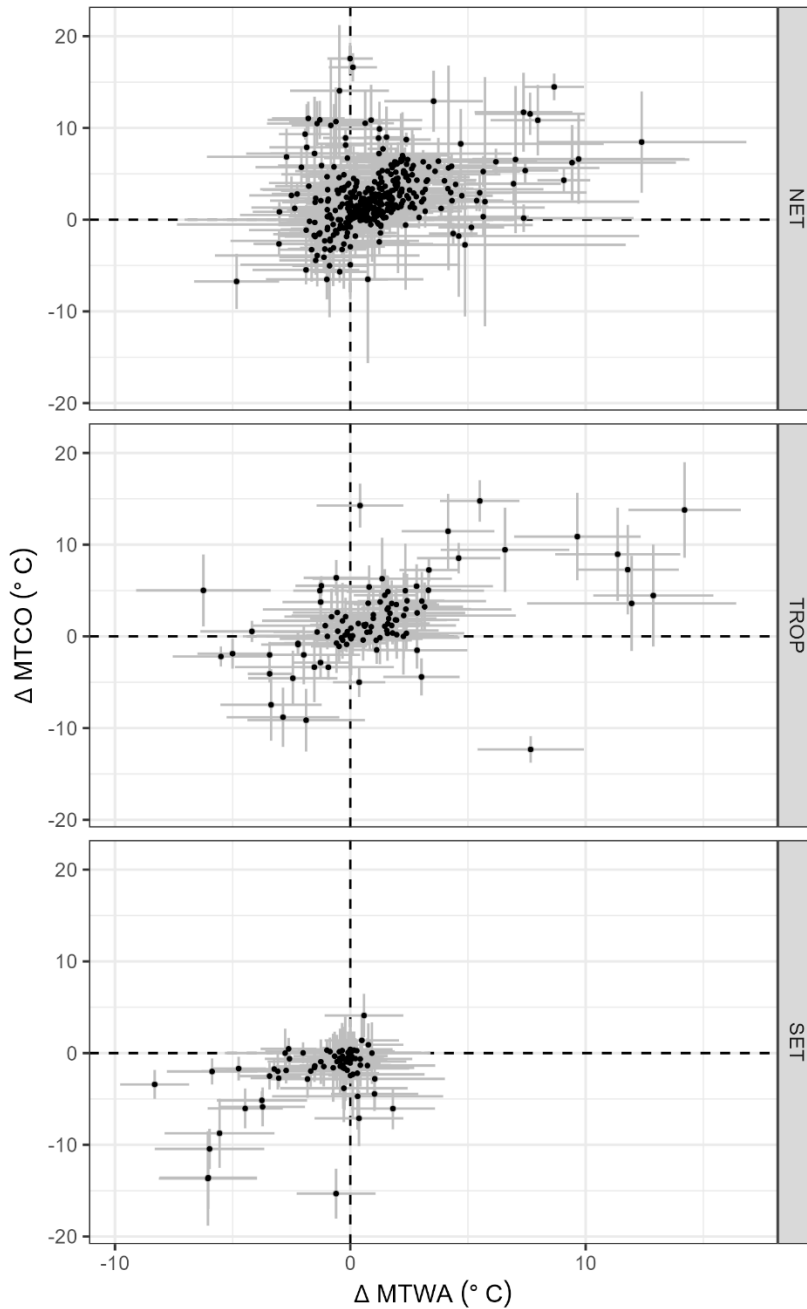
860

861

862

863

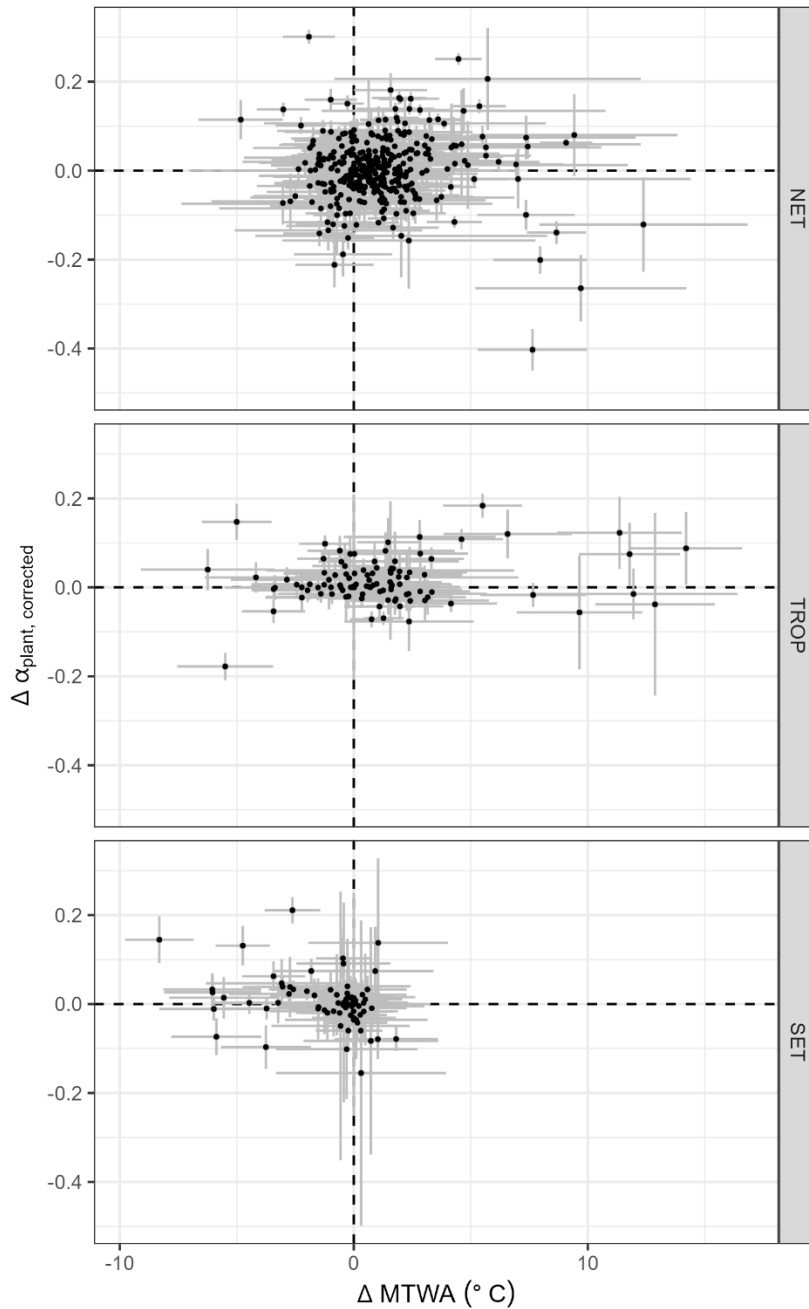
864 Figure 3: Scatter plot of the change in mean temperature of the coldest month (ΔMTCO) versus
865 the change in mean temperature of the warmest month (ΔMTWA) during individual
866 Dansgaard-Oeschger (D-O) events at individual sites. The points are grouped into the northern
867 extratropics (NET, north of 23.5°N), the tropics (TROP, between 23.5°N and 23.5°S) and the
868 southern extratropics (SET, south of 23.5°S). The grey lines indicate ± 1 error of the change.



869

870

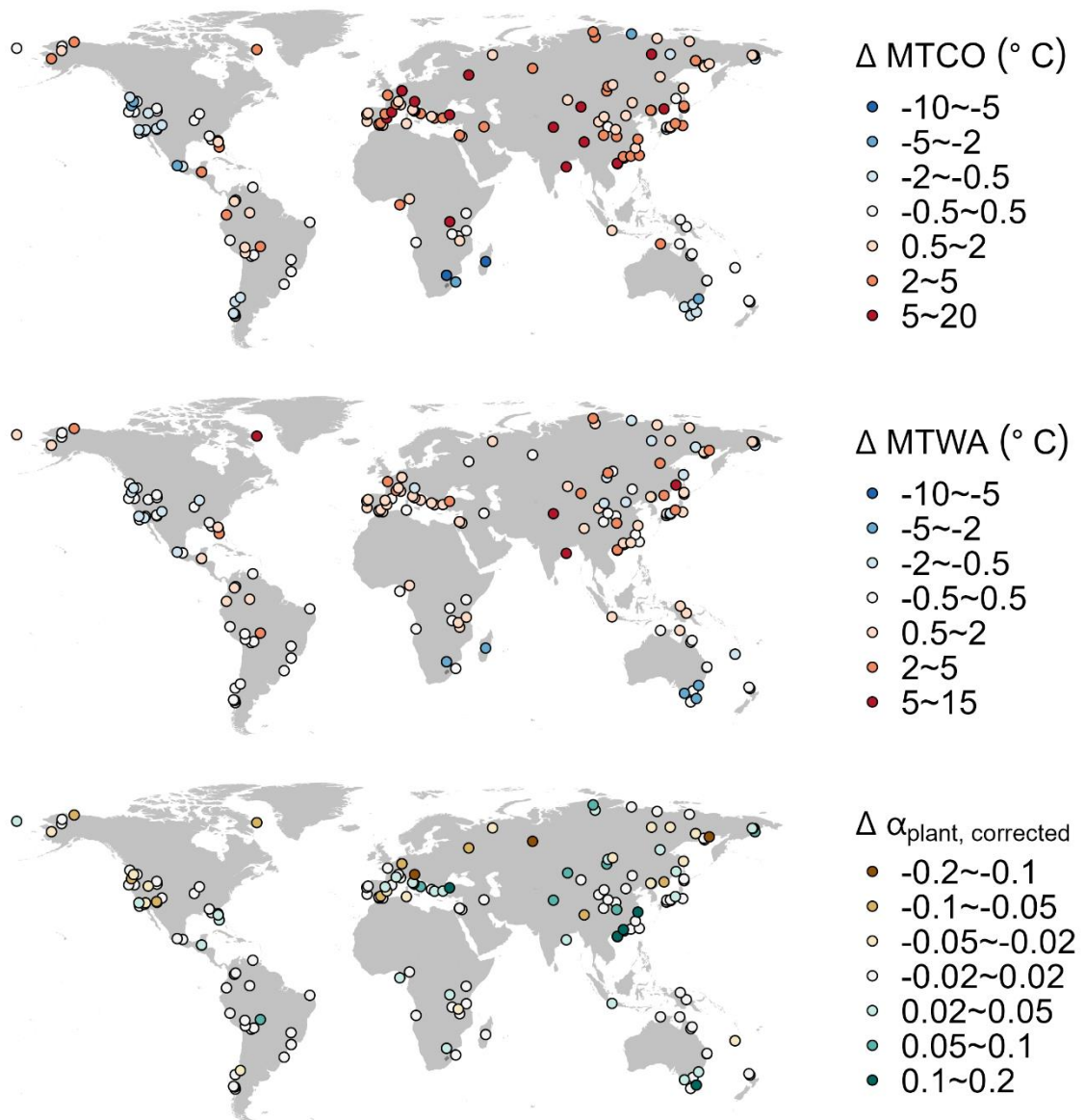
871 Figure 4: Scatter plot of the change in CO₂-corrected plant-available moisture ($\Delta\alpha_{\text{plant,corrected}}$)
872 versus the change in mean temperature of the warmest month (ΔMTWA) during individual
873 Dansgaard-Oeschger (D-O) events at individual sites. The points are grouped into the northern
874 extratropics (NET, north of 23.5°N), the tropics (TROP, between 23.5°N and 23.5°S) and the
875 southern extratropics (SET, south of 23.5°S). The grey lines indicate ± 1 error of the change.



876

877

878 Figure 5: Map showing the median change of site-based reconstructions for Dansgaard-
 879 Oeschger (D-O) events 5 to 12. The panels from top to bottom show the changes in mean
 880 temperature of the coldest month (ΔMTCO), mean temperature of the warmest month
 881 (ΔMTWA) and CO_2 -corrected plant-available moisture ($\Delta\alpha_{\text{plant,corrected}}$).

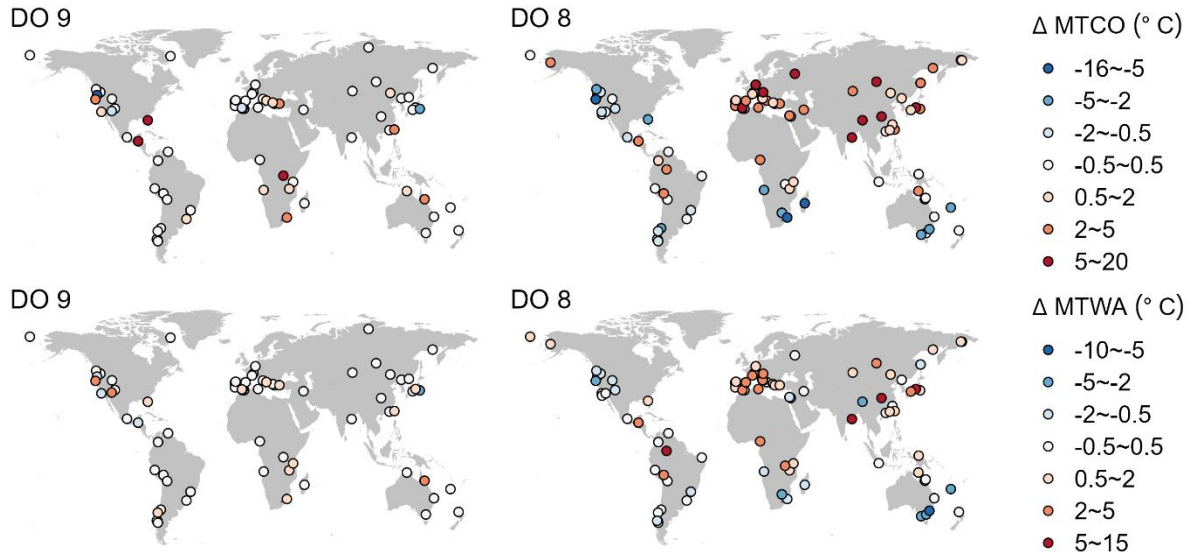


882

883

884

885 Figure 6: Map showing the change in mean temperature of the coldest month (ΔMTCO) and
 886 the change in mean temperature of the warmest month (ΔMTWA) for D-O 9 (a weak event)
 887 and D-O 8 (a strong event). The upper panel shows ΔMTCO , while the lower panel shows
 888 ΔMTWA .

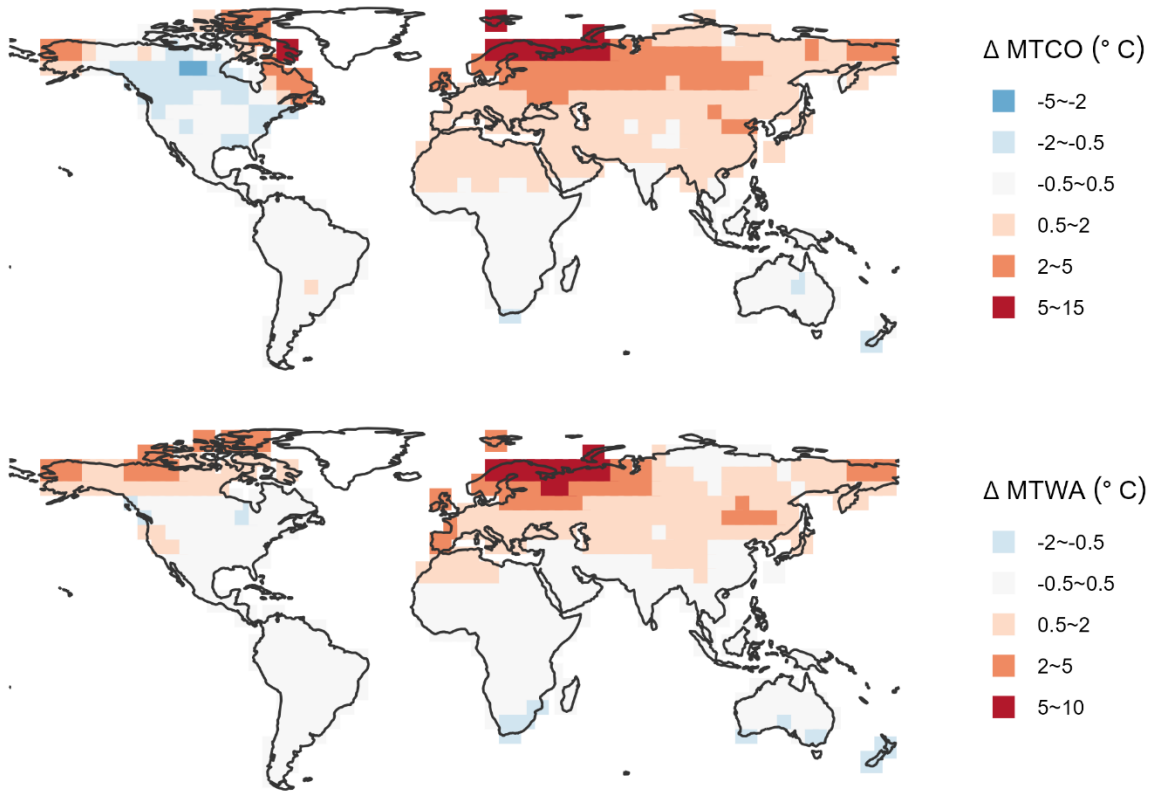


889

890

891

892 Figure 7: Map showing the median change of LOVECLIM simulations over (ice-free) land for
893 Dansgaard-Oeschger (D-O) events 5 to 12. The upper panel shows the change in mean
894 temperature of the coldest month (ΔMTCO), and the lower panel shows the change in mean
895 temperature of the warmest month (ΔMTWA).

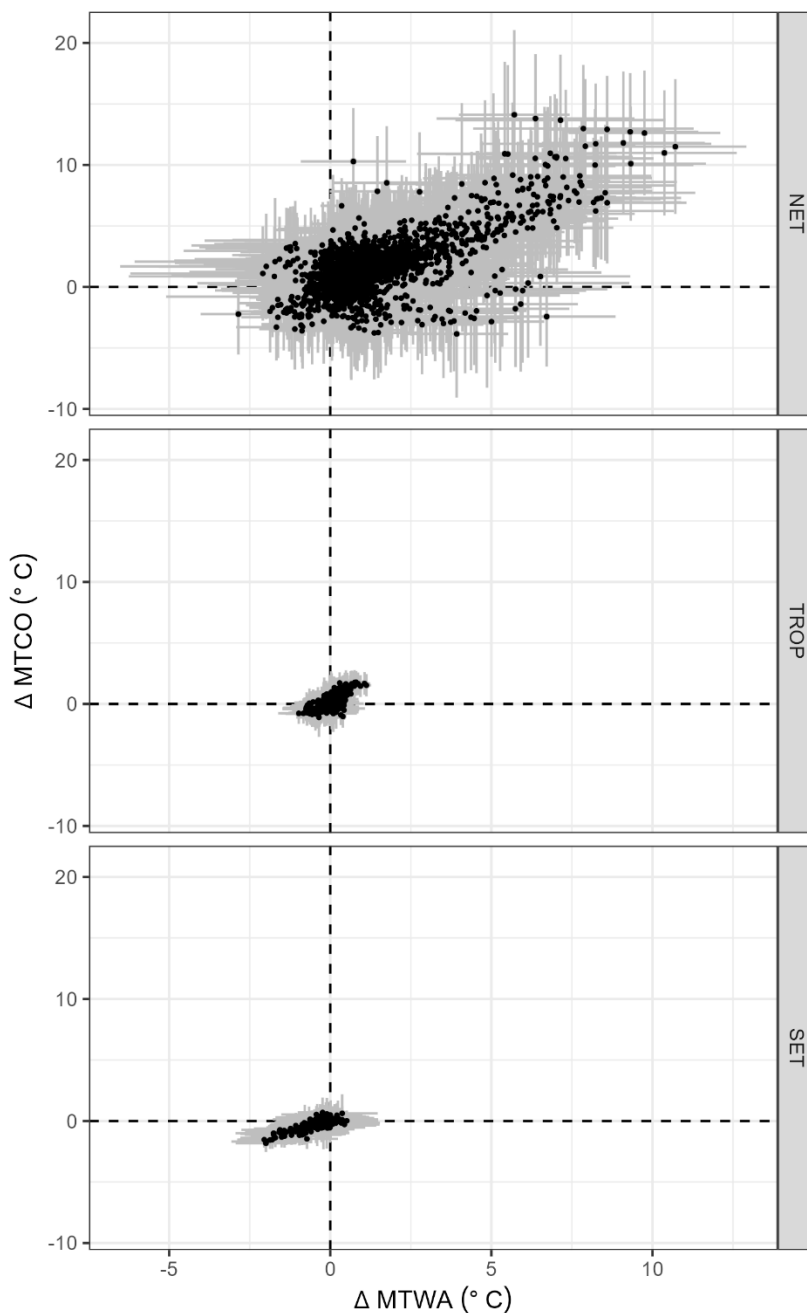


896

897

898

899 Figure 8: Scatter plot of the change in mean temperature of the coldest month (ΔMTCO) versus
900 the change in mean temperature of the warmest month (ΔMTWA) during individual
901 Dansgaard-Oeschger (D-O) events at individual (ice-free) land grids simulated by the
902 LOVECLIM model, using the same way to identify changes as the reconstructions. The points
903 are grouped into the northern extratropics (NET, north of 23.5°N), the tropics (TROP, between
904 23.5°N and 23.5°S) and the southern extratropics (SET, south of 23.5°S). The grey lines
905 indicate ± 1 error of the change.



906

907

908 Table 1: Site information of the fossil pollen records covering the interval 50-30 ka. The
 909 references with full citation are given in Supplementary Materials, section 3. lat is the latitude,
 910 lon is the longitude, elv is the elevation (unit: m). TERR means terrestrial record, MARI means
 911 marine record. n_{due} is the number of D-O events that should be found based on the time interval
 912 covered by the record. n_{miss} is the number of D-O events that were not identified. n_{low} is the
 913 number of D-O events missed because of low resolution of that part of the record. Some
 914 sites provide records in 50-30 ka but do not cover the intervals of the D-O events; some marine
 915 sites are too far from the land to extract GWR modern MTGR to apply CO₂ correction; these
 916 sites are all indicated by NA in n_{due} , n_{miss} and n_{low} .

name	lat	lon	elv	type	source	n_{due}	n_{miss}	n_{low}
Abric Romani	41.53	1.68	350	TERR	ACER	2	0	0
Akulinin Exposure P1282	47.12	138.55	20	TERR	Legacy2	1	0	0
Alut Lake	60.14	152.31	480	TERR	Cao et al. (2019, 2020)	7	1	1
Anderson Pond (ANDERSON)	36.03	-85.50	303	TERR	Legacy2	NA	NA	NA
Auel_AU2	50.28	6.59	457	TERR	AUTHOR	7	0	0
Aueler Maar ELSA AU3	50.28	6.60	456	TERR	Pangaea	3	0	0
Aueler Maar ELSA AU4	50.28	6.59	457	TERR	Pangaea	7	2	2
Azzano Decimo	45.88	12.72	10	TERR	ACER	4	0	0
Bajondillo	36.62	-4.50	20	TERR	Legacy2	2	0	0
Baldwin Lake	34.28	-116.81	2060	TERR	Legacy2	4	1	1
Balikun Lake	43.68	92.80	1575	TERR	Legacy2	NA	NA	NA
Balikun Lake BLK11A	43.68	92.80	1575	TERR	AUTHOR	2	0	0
Bambili 2	5.93	10.24	2323	TERR	Legacy2	5	1	1
Bandung DPDR-II	-6.99	107.73	662	TERR	Legacy2	4	2	2
Bay of Biscay	45.35	-5.22	-4100	MARI	Legacy2	NA	NA	NA
Bear Lake (BL00-1E)	41.95	-111.31	1805	TERR	ACER	7	2	2
Bereyekh River	63.28	147.75	800	TERR	Cao et al. (2019, 2020)	NA	NA	NA
Biggsville [Cessford Quarry]	40.86	-90.88	198	TERR	Legacy2	1	0	0
Bolotnyii Stream Exposure 117	42.85	132.78	4	TERR	Legacy2	2	1	1
Bolshoe Toko PG2133	56.04	130.87	903	TERR	Legacy2	2	0	0
Bolshoy Lyakhovsky Island	73.33	141.50	7	TERR	Legacy2	NA	NA	NA
Boney Spring	38.11	-93.37	210	TERR	Legacy2	1	1	1

Byllatskoye Exposure, Byllat River, Indigirka Basin	69.17	140.06	316	TERR	Legacy2	NA	NA	NA
Cala Conto	-17.57	-65.93	2700	TERR	Legacy2	2	2	2
Caledonia Fen	-37.33	146.73	1280	TERR	ACER	7	2	2
Cambara do Sul	-29.05	-50.10	1040	TERR	ACER	7	2	0
Camel Lake	30.26	-85.01	20	TERR	ACER	2	1	1
Carp Lake	45.91	-120.88	720	TERR	ACER	8	3	3
Changping CHZK1	40.18	116.22	49	TERR	Zhou et al. (2023)	NA	NA	NA
Chenghai CH2	23.48	116.80	5	TERR	Zhou et al. (2023)	4	1	1
Cheremushka Bog	52.75	108.08	1500	TERR	Cao et al. (2019, 2020)	1	0	0
Colonia	-23.87	-46.71	900	TERR	ACER	7	5	5
Colonia CO3	-23.87	-46.71	900	TERR	Legacy2	7	4	4
Core Trident 163 31B	-3.61	-83.96	-3210	MARI	ACER	NA	NA	NA
Correo	44.56	6.00	1100	TERR	Legacy2	1	0	0
Crystal Lagoon	-40.48	148.35	8	TERR	Legacy2	1	0	0
Daihai Lake-Wajianggou	40.58	112.67	1500	TERR	Zhou et al. (2023)	NA	NA	NA
Dajiu Lake DJH-1	31.49	110.00	1751	TERR	Zhou et al. (2023)	8	1	1
Dalai Nur Lake-Haiyan	43.28	116.58	1200	TERR	Zhou et al. (2023)	NA	NA	NA
Daluoba	47.83	88.20	2020	TERR	Zhou et al. (2023)	NA	NA	NA
Dar Fatma	36.82	8.77	780	TERR	Legacy2	7	2	2
Daxing DZK1	39.72	116.32	49	TERR	Zhou et al. (2023)	NA	NA	NA
Dead Sea	31.51	35.47	-428	TERR	Pangaea	6	0	0
Demyanskoye	59.50	69.50	65	TERR	Cao et al. (2019, 2020)	1	0	0
Deva-Deva	-7.12	37.62	2600	TERR	Legacy2	4	1	1
Diexi Lake	32.04	103.68	2334	TERR	Zhou et al. (2023)	2	0	0
Dikikh Olyenyeyii Lake	67.75	-178.83	300	TERR	Cao et al. (2019, 2020)	3	1	1
Eastern Niger Delta	4.55	6.43	0	TERR	Legacy2	NA	NA	NA
Elikchan 4 Lake	60.75	151.88	810	TERR	Cao et al. (2019, 2020)	3	1	1
Emanda	65.29	135.76	671	TERR	Legacy2	4	1	1
Enmynveem River (mammoth site)	68.17	165.93	400	TERR	Legacy2	NA	NA	NA
Enmynveem River1	68.17	165.93	400	TERR	Cao et al. (2019, 2020)	NA	NA	NA

Erlongwan Maar Lake	42.30	126.37	724	TERR	Zhou et al. (2023)	2	0	0
Ershilipu	36.93	116.65	50	TERR	Zhou et al. (2023)	NA	NA	NA
EW9504-17 PC	42.23	-125.81	-2671	MARI	ACER	NA	NA	NA
F2-92-P29	32.90	-119.73	-1475	MARI	ACER	2	2	2
Faddeyevskiy	75.33	143.83	30	TERR	Legacy2	NA	NA	NA
Fargher Lake	45.88	-122.58	200	TERR	ACER	8	2	1
Feng Suancigou Feng	35.51	105.81	1840	TERR	Zhou et al. (2023)	1	1	1
Fog Lake	67.18	-63.25	422	TERR	Legacy2	2	1	1
Fundo Nueva	-41.28	-73.83	66	TERR	ACER	5	1	0
Fuquene	5.45	-73.46	2540	TERR	ACER	7	3	3
Furamoos	47.98	9.88	662	TERR	ACER	NA	NA	NA
Gantang SZY	26.77	119.03	1007	TERR	Zhou et al. (2023)	5	1	1
GeoB2107-3	-27.18	-46.45	-1048	MARI	Legacy2	NA	NA	NA
GeoB3104	-3.67	-37.72	-767	MARI	ACER	1	1	1
Girraween Lagoon	-12.52	131.08	25	TERR	AUTHOR	5	1	1
Goshen Springs	31.72	-86.13	105	TERR	Legacy2	2	2	2
Grass Lake	41.65	-122.17	1537	TERR	Legacy2	3	0	0
Grays Lake (GRAYSG1)	43.07	-111.44	1195	TERR	Legacy2	4	1	1
Grays Lake (GRAYSG6)	43.07	-111.44	1195	TERR	Legacy2	NA	NA	NA
Guangzhou GZ-2	22.71	113.51	1	TERR	Zhou et al. (2023)	3	2	2
Guangzhou GZ-4	23.27	113.21	4	TERR	Zhou et al. (2023)	1	0	0
Gytgykai Lake	63.42	176.57	102	TERR	Cao et al. (2019, 2020)	1	0	0
Hachihama	34.55	133.95	6	TERR	Legacy2	3	1	1
Hangzhou HQB7	30.47	120.21	2	TERR	Zhou et al. (2023)	1	0	0
Hay Lake	34.00	-109.43	2780	TERR	ACER	NA	NA	NA
Headwaters Opasnaya River	48.23	138.48	1320	TERR	Legacy2	NA	NA	NA
Hosoike Moor	35.35	134.13	970	TERR	Legacy2	4	2	2
Huguangyan Maar Lake B	21.15	110.28	88	TERR	Zhou et al. (2023)	NA	NA	NA
Huinamarca (Lake Titicaca)	-16.23	-68.77	3810	TERR	ACER	3	0	0
Indigirka lowlands	70.58	145.00	20	TERR	Cao et al. (2019, 2020)	1	0	0
Ioannina	39.75	20.85	470	TERR	ACER	8	1	0
IODP Site 353-U1446A	19.08	85.73	-1430	MARI	Pangaea	6	1	1
Iwaya site	35.52	135.89	20	TERR	Legacy2	3	1	1

Jackson Pond (JACKSN07)	37.43	-85.72	260	TERR	Legacy2	NA	NA	NA
Jiangcun	34.40	109.50	650	TERR	Zhou et al. (2023)	3	0	0
Joe Lake	66.77	-157.22	183	TERR	ACER	3	1	1
Julietta Lake	61.34	154.56	880	TERR	Cao et al. (2019, 2020)	3	0	0
Kai Iwa	-35.82	173.65	70	TERR	AUTHOR	6	2	2
Kaiyak Lake	68.14	-161.44	190	TERR	Legacy2	NA	NA	NA
Kalaloch	47.63	-124.38	24	TERR	Legacy2	8	1	0
Kalistratikha	53.33	83.25	190	TERR	Cao et al. (2019, 2020)	NA	NA	NA
Kalistratikha Exposure	53.33	83.25	190	TERR	Legacy2	NA	NA	NA
Kamiyoshi Basin (KY01)	35.10	135.59	335	TERR	ACER	1	0	0
Kashiru Bog	-3.47	29.57	2240	TERR	ACER	NA	NA	NA
Kenbuchi Basin	44.05	142.38	135	TERR	ACER	3	0	0
Khoe	51.34	142.14	15	TERR	ACER	1	0	0
Khoe, Sakhalin Island	51.34	142.14	15	TERR	Cao et al. (2019, 2020)	4	2	2
Kirgirlakh Stream, Berelyekh River Basin (DIMA2)	62.67	147.98	700	TERR	Legacy2	NA	NA	NA
Kirgirlakh Stream, Berelyekh River Basin (DIMA3)	62.67	147.98	700	TERR	Legacy2	1	0	0
Kirgirlakh Stream_2	62.67	147.98	700	TERR	Cao et al. (2019, 2020)	1	1	1
Kohuora	-36.95	174.87	5	TERR	ACER	NA	NA	NA
Komanimambuno Mire	-5.82	145.09	2740	TERR	Legacy2	NA	NA	NA
Kunming Basin KZ2-3	25.00	102.62	1890	TERR	Zhou et al. (2023)	NA	NA	NA
Kupena (KUPENA3)	41.98	24.33	1356	TERR	Legacy2	NA	NA	NA
Kurota Lowland	35.52	135.88	20	TERR	ACER	1	0	0
KW31	3.52	5.57	-1181	MARI	ACER	1	0	0
La Laguna	4.92	-74.03	2900	TERR	ACER	1	0	0
Labaz lake (LAO6-95)	72.29	99.61	42	TERR	Legacy2	2	1	0
Lac du Bouchet - DIGI	44.83	3.82	1200	TERR	ACER	8	1	0
Lac Emeric	-22.30	166.97	230	TERR	Legacy2	3	1	1
Lac Suprin	-22.29	166.99	235	TERR	Legacy2	4	2	2
Lagaccione	42.57	11.80	355	TERR	ACER	3	0	0
Lago Grande di Monticchio	40.94	15.61	656	TERR	ACER	8	0	0
Lagoa Campestre de Salitre (SALILC3)	-19.00	-46.77	980	TERR	Legacy2	3	2	2
Lagoa das Patas	0.27	-66.68	300	TERR	Legacy2	4	1	1

Laguna Bella Vista	-13.62	-61.55	600	TERR	ACER	2	1	1
Laguna Chaplin	-14.47	-61.07	600	TERR	ACER	NA	NA	NA
Laguna Ciega	6.48	-72.39	3510	TERR	Legacy2	NA	NA	NA
Laguna Junin	-11.00	-76.17	4100	TERR	Legacy2	5	2	2
Lake Ailike	46.54	86.36	278	TERR	AUTHOR	5	0	0
Lake Albert (Lake Mobutu Sese Seko)	1.83	31.17	619	TERR	Legacy2	NA	NA	NA
Lake Annie	27.21	-81.35	34	TERR	Legacy2	1	0	0
Lake Baikal_BDP99	52.09	105.84	456	TERR	Pangaea	7	0	0
Lake Billyakh	65.28	126.78	340	TERR	ACER	3	0	0
Lake Biwa (BIW95-4)	35.25	136.05	84	TERR	ACER	3	0	0
Lake Carpentaria	-12.52	140.35	-60	MARI	Legacy2	4	2	2
Lake Chalco CHA08	19.25	-98.97	2250	TERR	AUTHOR	5	1	1
Lake Consuelo (CON1)	-13.95	-68.99	1360	TERR	ACER	7	2	2
Lake E5	68.64	-149.46	803	TERR	Legacy2	NA	NA	NA
Lake Elsinore	33.66	-117.35	376	TERR	Legacy2	1	0	0
Lake Fimon	45.47	11.53	23	TERR	AUTHOR	NA	NA	NA
Lake George	-35.09	149.43	673	TERR	Legacy2	4	0	0
Lake Hordorli	-2.54	140.59	798	TERR	Legacy2	4	0	0
Lake Iznik	40.43	29.53	88	TERR	Legacy2	1	0	0
Lake Malawi	-11.22	34.42	470	TERR	ACER	5	2	2
Lake Masoko	-9.33	33.75	840	TERR	ACER	2	1	1
Lake Nero (NERO2)	57.18	39.45	93	TERR	Legacy2	NA	NA	NA
Lake Nojiri	36.83	138.22	657	TERR	ACER	8	0	0
Lake Patzcuaro	19.58	-101.58	2044	TERR	Legacy2	2	1	1
Lake Peten-Itza	16.99	-89.82	110	TERR	Legacy2	8	1	1
Lake Quexil	16.92	-89.82	110	TERR	Legacy2	4	2	2
Lake Selina	-41.88	145.61	516	TERR	Legacy2	1	0	0
Lake Tanganyika (KH3)	-8.50	30.75	773	TERR	Legacy2	4	2	2
Lake Tanganyika (KH4)	-8.50	30.75	773	TERR	Legacy2	NA	NA	NA
Lake Tanganyika [north basin] (SD24TAN)	-4.19	29.31	773	TERR	Legacy2	NA	NA	NA
Lake Tritrivakely	-19.78	46.92	1778	TERR	Legacy2	5	1	0
Lake Tulane	29.83	-81.95	36	TERR	ACER	7	1	1
Lake Wangoom LW87 core	-38.35	142.60	100	TERR	ACER	4	0	0
Lake Xinias	39.05	22.27	500	TERR	ACER	8	3	3
Lake Yamozero	65.02	50.23	213	TERR	Legacy2	2	0	0
Lake Zeribar	35.53	46.12	1288	TERR	Legacy2	7	1	1
Ledovyi Obryv Exposure, Northern Section	64.10	171.18	57	TERR	Legacy2	NA	NA	NA
Les Echets G - DIGI	45.90	4.93	267	TERR	ACER	8	0	0
Levantine Basin	32.03	34.28	0	TERR	Legacy2	4	1	1

Levinson Lessing Lake PG1228	74.47	98.64	47	TERR	Cao et al. (2019, 2020)	1	0	0
Little Lake	44.16	-123.58	217	TERR	ACER	5	0	0
Lop Nur K1	40.28	90.25	780	TERR	Zhou et al. (2023)	NA	NA	NA
Luanhaizi Lake LH2	37.59	101.35	3200	TERR	Zhou et al. (2023)	1	0	0
Luochuan	35.75	109.42	1068	TERR	Zhou et al. (2023)	NA	NA	NA
Lynchs Crater	-17.37	145.70	760	TERR	ACER	7	4	4
Malyi Krechet Lake	64.80	175.53	32	TERR	Legacy2	2	0	0
Mamontovy Khayata	71.77	129.45	0	TERR	Cao et al. (2019, 2020)	3	0	0
Mamontovy Klyk	73.61	117.13	25	TERR	Legacy2	1	0	0
MD01-2421	36.02	141.77	-2224	MARI	ACER	8	1	0
MD03-2622 Cariaco Basin	10.71	-65.17	-877	MARI	ACER	7	5	3
MD04-2845	45.35	-5.22	-4100	MARI	ACER	NA	NA	NA
MD84-629	32.07	34.35	-745	MARI	ACER	5	1	1
MD95-2039	40.58	-10.35	-3381	MARI	ACER	8	1	1
MD95-2042	37.80	-10.17	-3148	MARI	ACER	8	1	1
MD95-2043	36.14	-2.62	-1841	MARI	ACER	8	1	1
MD99-2331	41.15	-9.68	-2110	MARI	ACER	7	1	1
Megali Limni	39.10	26.32	323	TERR	ACER	6	0	0
Melkoye Lake	64.86	175.23	36	TERR	Cao et al. (2019, 2020)	1	0	0
Mereya River	46.62	142.92	4	TERR	Cao et al. (2019, 2020)	NA	NA	NA
Mfabeni Peatland	-28.15	32.52	11	TERR	ACER	4	1	0
Middle Butte Cave	43.37	-112.62	1590	TERR	Legacy2	NA	NA	NA
Milin	29.31	94.35	2982	TERR	Zhou et al. (2023)	3	0	0
Moershoofd	51.25	3.52	2	TERR	Legacy2	NA	NA	NA
Morro de Itapeva	-22.78	-45.53	1850	TERR	Legacy2	NA	NA	NA
Mud Lake (MUDLAKE)	29.30	-81.87	9	TERR	Legacy2	4	1	1
Muscotah Marsh	39.53	-95.51	280	TERR	Legacy2	NA	NA	NA
Nachtigall	51.81	9.40	95	TERR	Legacy2	NA	NA	NA
Nakafurano	43.37	142.43	173	TERR	ACER	2	1	1
Native Companion Lagoon	-27.68	153.41	20	TERR	ACER	4	2	2
Navarres	39.10	-0.68	225	TERR	ACER	3	0	0
Ngamakala Pound (GAMA4)	-4.08	15.38	400	TERR	Legacy2	NA	NA	NA
Ngoring Lake CK6	34.92	97.73	4272	TERR	Zhou et al. (2023)	NA	NA	NA

Noordzee T121	54.10	4.21	0	TERR	Legacy2	NA	NA	NA
Northern Coast of Onemen Gulf	64.78	176.17	18	TERR	Legacy2	3	0	0
ODP 1233 C	-41.00	-74.45	-838	MARI	ACER	8	2	1
ODP 1234	-36.22	-73.68	-1015	MARI	ACER	8	0	0
ODP 820	-16.63	146.30	-280	MARI	ACER	5	3	3
ODP site 976	36.20	-4.30	-1108	MARI	ACER	8	1	0
ODP1019	41.66	-124.91	989	MARI	ACER	7	3	3
ODP1078C	-11.92	13.40	-426	MARI	ACER	8	2	1
ODP893A	34.28	-120.03	-577	MARI	ACER	8	0	0
Oil Lake	70.29	-151.17	745	TERR	Legacy2	2	0	0
Okarito Pakihi	-43.24	170.22	70	TERR	ACER	NA	NA	NA
Ovrazhnyi Stream-2	43.25	134.57	10	TERR	Cao et al. (2019, 2020)	NA	NA	NA
Ovrazhnyii-1 Stream Exposure	43.25	134.57	8	TERR	Legacy2	NA	NA	NA
Ovrazhnyii-2 Exposure 667-842	43.25	134.57	10	TERR	Legacy2	NA	NA	NA
Padul	37.01	-3.60	726	TERR	AUTHOR	6	2	2
Paramonovskii Stream	43.20	133.75	120	TERR	Cao et al. (2019, 2020)	NA	NA	NA
Paramonovskii Stream Exposure 4980	43.20	133.75	120	TERR	Legacy2	NA	NA	NA
Pavlovka Exposure 988	44.32	134.00	300	TERR	Legacy2	NA	NA	NA
Peloncillo Mountains	32.29	-109.09	1400	TERR	Legacy2	NA	NA	NA
Peschanka Exposure 155	43.30	132.12	12	TERR	Legacy2	NA	NA	NA
Pittsburg Basin	38.90	-89.19	162	TERR	Legacy2	NA	NA	NA
Pleshevo Lake	56.77	38.78	148	TERR	Legacy2	2	0	0
Potato Lake	34.45	-111.33	2222	TERR	ACER	1	1	1
Poutu	-36.38	174.13	82	TERR	AUTHOR	1	1	1
Pretoria Saltpan	-25.41	28.08	1150	TERR	Legacy2	4	0	0
Qingdao ZK2	36.29	120.46	31	TERR	Zhou et al. (2023)	NA	NA	NA
Qingdao ZK3	36.26	120.64	7	TERR	Zhou et al. (2023)	NA	NA	NA
Rahue	-39.37	-70.93	1000	TERR	Legacy2	NA	NA	NA
Reenadinna Wood	52.01	-9.53	20	TERR	Legacy2	NA	NA	NA
Rice Lake (Rice Lake 81)	40.30	-123.22	1100	TERR	ACER	NA	NA	NA
Rietvlei-Still Bay	-34.35	21.54	17	TERR	Legacy2	NA	NA	NA
Rio Timbio	2.37	-76.71	1750	TERR	Legacy2	NA	NA	NA
Rockyhock Bay	36.17	-76.68	6	TERR	Legacy2	NA	NA	NA
Ruby Marsh	41.13	-115.51	1818	TERR	Legacy2	1	0	0
Rusaka Swamp	-3.43	29.62	2070	TERR	Legacy2	1	0	0
Sacred Lake	0.05	37.53	2345	TERR	Legacy2	3	2	2
Saint-Ursin	48.52	-0.25	234	TERR	Legacy2	3	0	0

San Agustin Plains (SAPBHM)	33.87	-108.25	2069	TERR	Legacy2	NA	NA	NA
Sangluoshu	37.50	117.73	50	TERR	Zhou et al. (2023)	NA	NA	NA
Sanshui K5	22.78	112.63	12	TERR	Zhou et al. (2023)	NA	NA	NA
Shaamar	50.20	105.20	650	TERR	Legacy2	2	0	0
Shuidonggou SDG2	38.28	106.50	1200	TERR	Zhou et al. (2023)	NA	NA	NA
Shunyi GZK1	40.15	116.53	50	TERR	Zhou et al. (2023)	NA	NA	NA
Siberia	-17.09	-64.72	2920	TERR	ACER	1	1	1
Siberia1	-17.09	-64.72	2920	TERR	Legacy2	1	1	1
Sihailongwan Maar Lake	42.28	126.60	797	TERR	Pangaea	8	1	1
Siluyanov Yar-2 Exposure	46.13	137.83	25	TERR	Legacy2	NA	NA	NA
Sirunki Wabag	-5.44	143.53	2550	TERR	Legacy2	2	0	0
St. Catherines Island (Northwest Marsh)	31.69	-81.15	0	TERR	Legacy2	NA	NA	NA
Stoneman Lake_STL	34.78	-111.52	2048	TERR	AUTHOR	3	0	0
Stracciacappa	42.13	12.32	220	TERR	ACER	4	0	0
Straldzha mire (QUARRY)	42.63	26.78	137	TERR	Legacy2	NA	NA	NA
Tagua Tagua - DIGI	-34.50	-71.16	200	TERR	ACER	6	1	1
Taiquemo	-42.17	-73.60	170	TERR	ACER	8	0	0
Tanon River	59.67	151.20	40	TERR	Cao et al. (2019, 2020)	NA	NA	NA
Tanon River [Quarry Site]	59.67	151.20	40	TERR	Legacy2	NA	NA	NA
Taymyr Lake SAO1	74.55	100.53	47	TERR	Cao et al. (2019, 2020)	NA	NA	NA
Tianshuihai TS95	35.35	79.52	4900	TERR	Zhou et al. (2023)	1	0	0
Tianyang Maar Lake TYC	20.52	110.30	108	TERR	Zhou et al. (2023)	3	0	0
Tianyang TY1	20.35	110.35	90	TERR	Zhou et al. (2023)	1	1	0
Tikhangou Exposure	42.83	132.78	4	TERR	Legacy2	NA	NA	NA
Toadlena Lake [Dead Man Lake] (DEAD5826)	36.24	-108.95	2759	TERR	Legacy2	1	0	0
Toadlena Lake [Dead Man Lake] (DEAD6101)	36.24	-108.95	2759	TERR	Legacy2	4	2	2
Tortoise Lagoon	-27.52	153.47	39	TERR	Legacy2	2	2	2
Toushe Basin	23.82	120.88	650	TERR	ACER	8	0	0
Toushe Lake 2013	23.82	120.88	650	TERR	Zhou et al. (2023)	1	0	0
Tswaing Crater	-25.40	28.08	1100	TERR	ACER	5	0	0

Tukuto Lake	68.50	-157.03	505	TERR	Legacy2	1	1	1
Tyrrendara Swamp	-38.20	141.76	13	TERR	ACER	NA	NA	NA
Ulan Buh Desert WL10ZK-1	40.04	105.78	1026	TERR	Zhou et al. (2023)	NA	NA	NA
Valle di Castiglione	41.90	12.76	44	TERR	ACER	7	3	3
Villarquemado	40.82	-1.48	985	TERR	AUTHOR	4	1	0
Vinillos	-0.60	-77.85	2090	TERR	Legacy2	1	0	0
Voordrag	-27.74	31.33	940	TERR	Legacy2	NA	NA	NA
W8709-13 PC	42.11	-125.75	-2712	MARI	ACER	NA	NA	NA
W8709-8 PC	42.26	-127.68	-3111	MARI	ACER	NA	NA	NA
Walker Lake	35.38	-111.71	2500	TERR	ACER	NA	NA	NA
Wenquangou	35.92	94.20	4700	TERR	Zhou et al. (2023)	NA	NA	NA
White Pond (WHITESC)	34.17	-80.78	90	TERR	Legacy2	NA	NA	NA
Wulagai Lake	45.42	117.48	822	TERR	AUTHOR	7	0	0
Xere Wapo	-22.30	166.96	235	TERR	Legacy2	NA	NA	NA
Xijir Ulan Lake	35.23	90.33	4500	TERR	Zhou et al. (2023)	NA	NA	NA
Xining ZK2	35.97	101.67	4363	TERR	Zhou et al. (2023)	NA	NA	NA
Yabulai Mt	39.62	103.92	1266	TERR	Zhou et al. (2023)	2	0	0
Yangerzhuang	38.35	117.35	5	TERR	Zhou et al. (2023)	NA	NA	NA
Yangjiapo	40.02	118.68	70	TERR	Zhou et al. (2023)	NA	NA	NA
Yangyuan-Caocun	40.10	114.40	875	TERR	Zhou et al. (2023)	1	0	0
Yaxi Co Lake	34.28	92.67	4000	TERR	Zhou et al. (2023)	NA	NA	NA
Zagoskin Lake	63.45	-162.11	7	TERR	Legacy2	5	0	0
Zhongshan PK19	21.80	113.30	6	TERR	Zhou et al. (2023)	NA	NA	NA

917

918

919 Table 2: Leave-out cross-validation (with geographically and climatically close sites removed)
 920 using fxTWA-PLSv2, for mean temperature of the coldest month (MTCO), mean temperature
 921 of the warmest month (MTWA) and plant-available moisture (α_{plant}). P-splines smoothed \hat{f}_x was
 922 estimated using 200 bins. n is the number of components used; Avg.bias is the average bias;
 923 RMSEP is the root-mean-square error of prediction; $\Delta\text{RMSEP}\%$ is the per cent change of
 924 RMSEP of the current number of components compared to using one component less, i.e. 100
 925 $\times (\text{RMSEP}_n - \text{RMSEP}_{n-1}) / \text{RMSEP}_{n-1}$. The p value assesses whether using the current number
 926 of components represents a significant ($p \leq 0.01$) difference over using one fewer component.
 927 To avoid over-fitting, the last significant number of components (i.e. the first insignificant
 928 number of components minus 1; p can become significant again after being insignificant with
 929 increasing n , but regarded meaningless) is selected for subsequent analyses and indicated in
 930 **bold**. The degree of overall compression is assessed by linear regression of the cross-validated
 931 reconstructions against the variable; b_1 and σ_{b_1} are the slope and the standard error of the slope,
 932 respectively. A slope (b_1) of 1 indicates no compression.

	n	R^2	Avg.bias	RMSEP	$\Delta\text{RMSEP}\%$	p	b_1	σ_{b_1}
MTCO (°C)	1	0.72	-1.15	6.89	NA	NA	0.82	0.00
	2	0.73	-1.25	6.75	-2.00	0.001	0.83	0.00
	3	0.74	-1.20	6.66	-1.42	0.001	0.84	0.00
	4	0.74	-1.23	6.66	0.02	0.663	0.84	0.00
	5	0.74	-1.24	6.64	-0.31	0.001	0.84	0.00
	6	0.74	-1.24	6.63	-0.11	0.001	0.84	0.00
MTWA (°C)	1	0.51	-0.32	4.00	NA	NA	0.64	0.00
	2	0.59	-0.22	3.67	-8.32	0.001	0.72	0.00
	3	0.60	-0.25	3.63	-0.95	0.001	0.72	0.00
	4	0.60	-0.25	3.62	-0.29	0.012	0.72	0.00
	5	0.60	-0.27	3.63	0.22	0.974	0.72	0.00
	6	0.60	-0.28	3.61	-0.61	0.001	0.72	0.00
α_{plant}	1	0.61	-0.020	0.191	NA	NA	0.65	0.00
	2	0.62	-0.022	0.190	-0.49	0.001	0.67	0.00
	3	0.63	-0.020	0.186	-2.07	0.001	0.68	0.00
	4	0.64	-0.020	0.186	-0.30	0.020	0.69	0.00
	5	0.64	-0.020	0.185	-0.18	0.003	0.70	0.00
	6	0.64	-0.020	0.185	0.09	0.988	0.70	0.00

933

934

935 Table 3: Maximum likelihood estimates of the relationship between the change in mean
 936 temperature of the coldest month (ΔMTCO) and the change in mean temperature of the
 937 warmest month (ΔMTWA) for the northern extratropics (NET, north of 23.5°N), tropics
 938 (TROP, between 23.5°N and 23.5°S) and southern extratropics (SET, south of 23.5°S). The
 939 intercepts were set to zero since both variables are changes.

Region		Coefficient	Standard error (SE)	Lower 95%	Upper 95%
NET	Slope	2.9	0.5	2.0	3.8
TROP	Slope	2.1	0.4	1.2	3.0
SET	Slope	1.5	0.7	0.2	2.8

940

941

942 Table 4: Maximum likelihood estimates of the relationship between the change in CO₂-
 943 corrected plant-available moisture ($\Delta\alpha_{\text{plant,corrected}}$) and the change in mean temperature of the
 944 warmest month (ΔMTWA) for the northern extratropics (NET, north of 23.5°N), tropics
 945 (TROP, between 23.5°N and 23.5°S) and southern extratropics (SET, south of 23.5°S). The
 946 intercepts were set to zero since both variables are changes.

Region		Coefficient	Standard error (SE)	Lower 95%	Upper 95%
NET	Slope	0.27	0.24	-0.21	0.74
TROP	Slope	0.02	0.01	0.01	0.04
SET	Slope	-0.03	0.02	-0.06	0.01

947

948

949 Table 5: Maximum likelihood estimates of the relationship between the change in mean
 950 temperature of the coldest month (ΔMTCO) and the change in mean temperature of the
 951 warmest month (ΔMTWA) over (ice-free) land in LOVECLIM simulations, for the northern
 952 extratropics (NET, north of 23.5°N), tropics (TROP, between 23.5°N and 23.5°S) and southern
 953 extratropics (SET, south of 23.5°S). The intercepts were set to zero since both variables are
 954 changes.

Region		Coefficient	Standard error (SE)	Lower 95%	Upper 95%
NET	Slope	1.15	0.02	1.11	1.2
TROP	Slope	1.34	0.05	1.25	1.44
SET	Slope	0.76	0.03	0.70	0.81

955

956